Global fits of new physics in $b \to s$ after the $R_{K^{(*)}}$ 2022 release

Qiaoyi Wen and Fanrong Xu*

Department of Physics and Siyuan Laboratory, Jinan University, Guangzhou 510632, People's Republic of China

(Received 7 June 2023; accepted 28 October 2023; published 22 November 2023)

The measurement of lepton universality parameters $R_{K^{(*)}}$ was updated by LHCb in December 2022, which indicated that the well-known anomalies in flavor-changing neutral current (FCNC) processes of B meson decays have faded away. However, does this mean that all new physics possibilities related to $b \to s\ell^+\ell^-$ have been excluded? We aim to answer this question in this work. The state-of-the-art effective Hamiltonian is adopted to describe $b \to s$ transition, while BSM (beyond the Standard Model) new physics effects are encoded in Wilson coefficients (WCs). Using around 200 observables in leptonic and semileptonic decays of B mesons and bottom baryons, measured by LHCb, CMS, ATLAS, Belle, and *BABAR*, we perform global fits of these Wilson coefficients in four different scenarios. In particular, lepton flavors in WCs are specified in some of the working scenarios. To see the change of new physics parameters, we use both the data before and after the 2022 release of $R_{K^{(*)}}$ in two separate sets of fits. We find that in three of the four scenarios, ΔC_9^μ still has a deviation around or more than 4σ from the Standard Model. The lepton flavor in WCs is distinguishable for ΔC_9 at the 1σ level, but at the 2σ level all the operators are flavor identical. We demonstrate numerically that there is no chirality for muon type of scalar operator and it is kept at the 1σ level for their electron type dual ones, while chiral difference exists for $\mathcal{O}_9^\mu$ at least at the 2σ level. Moreover, it can be deduced that the scalar operators $\mathcal{O}_{S,P}^{(\prime)\mu}$ become null if new physics emerges in terms of Standard Model effective field theory (SMEFT) up to dimension-6.

DOI: 10.1103/PhysRevD.108.095038

I. INTRODUCTION

The quest for new physics in FCNC process $b \to s\ell^+\ell^-$ has lasted for more than one decade. It was expected that in $B \to K^*\mu^+\mu^-$ new physics effect would emerge by measuring the forward-backward asymmetry (AFB), and the early measurements carried out by Belle [1], *BABAR* [2] and CDF [3] indeed seemed to prefer the new physics with a flipped C_7. In 2011, however, a SM-like behavior of AFB was confirmed by LHCb even with its 309 pb^{-1} data [4]. Later on, more observables, including branching fractions, angular distributions and lepton universality parameters, were measured more and more precisely and deviations from SM predictions in particular bins were found by Belle [5–7], LHCb [8–16], ATLAS [17] and CMS [18,19].

The nonuniversality of lepton flavor, characterized by $R_{K^{(*)}} \equiv \mathcal{B}(B \to K^{(*)}\mu^+\mu^-)/\mathcal{B}(B \to K^{(*)}e^+e^-)$, is among one of the anomalies appearing in semileptonic B meson decays. The 2.6σ deviation of R_K in charged B meson decay was firstly reported in 2014 [8] and updated in 2019 [9] by LHCb. It was found by Belle in 2019 that a similar 2.6σ standard deviation also occurred at $q^2 \in (1.0, 6.0)\ \text{GeV}^2/c^4$ [6]. Later in 2021, with Run I and Run II dataset LHCb reported $R_K = 0.846^{+0.042}_{-0.039}(\text{stat})^{+0.013}_{-0.012}(\text{sys})$ as well as $R_{K_S} = 0.66^{+0.20}_{-0.14}(\text{stat})^{+0.02}_{-0.04}(\text{sys})$ at the level of 3.1σ and 1.5σ, respectively. As for $B \to V\ell^+\ell^-$ sector, in 2017 LHCb found 2.1–2.3σ and 2.4–2.5σ deviations for low-q^2 bins and central-q^2 bins in neutral B decay $B^0 \to K^{*0}\ell^+\ell^-$ [12]. Later in 2021, in charged B decay $B^+ \to K^{*+}\ell^+\ell^-$ LHCb reported its measurement as $R_{K^{*+}} = 0.70^{+0.18}_{-0.13}(\text{stat})^{+0.03}_{-0.04}(\text{sys})$, which only deviated by 1.4σ [11]. And a SM consistent results was also obtained by Belle in 2019 [5]. At the end of 2022, LHCb reported its updated measurement of $R_{K^{(*)}}$ at both low-q^2 and central-q^2 region by correcting previous underestimations on electron mode contribution [20], giving

$$\begin{aligned}
\text{low-}q^2 &\begin{cases} R_K = 0.994^{+0.090}_{-0.082}(\text{stat})^{+0.029}_{-0.027}(\text{syst}) \\ R_{K^*} = 0.927^{+0.093}_{-0.087}(\text{stat})^{+0.036}_{-0.035}(\text{syst}), \end{cases} \\
\text{central-}q^2 &\begin{cases} R_K = 0.949^{+0.042}_{-0.041}(\text{stat})^{+0.022}_{-0.022}(\text{syst}) \\ R_{K^*} = 1.027^{+0.072}_{-0.068}(\text{stat})^{+0.027}_{-0.026}(\text{syst}). \end{cases}
\end{aligned} \tag{1}$$

*fanrongxu@jnu.edu.cn

The overall 0.2σ deviation, compatible with SM, indicates that the expected new physics in form of lepton flavor nonuniversality has faded away. Regarding to the existence of several deviations in branching fractions and angular distribution, the remaining new physics opportunities in the $b \to s\ell^+\ell^-$ window are naturally of great interest. Therefore, it is timely to carry out updated global fits in combination with all the related data to help to understand current status.

So far there have been rich data on leptonic decay $B_{s,d} \to \ell^+\ell^-$ and semileptonic decay $B \to K\ell^+\ell^-$, $B \to K^*\ell^+\ell^-$, $B \to X_s\ell^+\ell^-$, $\Lambda_b \to \Lambda\ell^+\ell^-$. We collect all available observables of them as parts of inputs in fitting analysis. As for theoretical description, we adopt the state-of-the-art effective Hamiltonian, in which high energy particles are integrated out and absorbed in Wilson coefficients (WCs). In SM, there are only four effective operators contributed in the $b \to s\ell^+\ell^-$ effective Hamiltonian. New physics effects are brought in either by extra operators (the dual operators as well as scalar operators, see Sec. II) or modifications of WCs. At hadron energy scale, we rely on QCDF approach to deal with B meson semileptonic decays [21,22]. To extend our exploration in model-independent analysis, the global fits of four different cases with particular operator combinations are performed based on Bayesian statistics, taking into account both theoretical and experimental errors. Especially, the fit based on 20-D WCs by specifying lepton flavors as one of the working scenarios is provided. We make the fits both before and after the 2022 $R_{K^{(*)}}$ release, and make comparisons with some of the similar model-independent analyses done by other groups [23–29]. Although WCs slightly differ from each other in our four scenarios, we find commonly for ΔC_9^μ the around 4σ deviation from SM still exists after the 2022 $R_{K^{(*)}}$ release, which indicates that the new physics opportunity cannot be excluded. Meanwhile, we find that, at 1σ level, ΔC_{10}^μ is indistinguishable from ΔC_{10}^e but $\Delta C_{9,S,P}^\mu$ differ from $\Delta C_{9,S,P}^e$. The WCs $\Delta C_{S,P}^\mu$ are strictly chirality independent, while the equivalence between $\Delta C_{S,P}^e$ and $\Delta C_{S,P}^{\prime e}$ is obeyed at 1σ level. It can be demonstrated numerically that $\Delta C_{9,10}$ violate this chirality identity at least at 2σ level. By combining the data, we also find that scalar operators become null if the new physics is described within the framework of SMEFT.

The remaining parts of the paper are organized as follows. In Sec. II, we provide the whole working frame of the analysis, including theoretical framework of effective Hamiltonian approach and the adopted four different working scenarios (denoted as the muon-specific scenario, lepton-universal scenario, lepton-specific scenario and the full scenario), the related observables in all the involved decay processes as well as the fitting schemes. Then numerical analysis is given in Sec. III, with inputs summarized in III A, results presented in III B and discussions carried on in III C. We conclude the paper in Sec. IV. More details on theoretical formulas and experimental inputs can be referred to Appendix A and B, respectively.

II. THE WORKING FRAME

A. Theoretical framework

The state-of-the-art effective Hamiltonian is adopted to describe $b \to s$ transition, in which high energy information is contained in Wilson coefficients while remaining low energy part resorted to effective operators and their corresponding matrix elements. The Wilson coefficients can be obtained at electroweak scale by integrating out heavy particles and running into B meson scale with RGE, leading to the effective Hamiltonian

$$\mathcal{H} = -\frac{4G_F}{\sqrt{2}} V_{tb} V_{ts}^* \frac{e^2}{16\pi^2} \sum_i (C_i \mathcal{O}_i + C_i' \mathcal{O}_i') + \text{H.c.}, \qquad (2)$$

in which the effective operators are defined as

$$\begin{aligned}
\mathcal{O}_7 &= \frac{m_b}{e}(\bar{s}\sigma_{\mu\nu}P_R b)F^{\mu\nu}, & \mathcal{O}_7' &= \frac{m_b}{e}(\bar{s}\sigma_{\mu\nu}P_L b)F^{\mu\nu},\\
\mathcal{O}_8 &= \frac{g_s m_b}{e^2}(\bar{s}\sigma_{\mu\nu}T^a P_R b)G_a^{\mu\nu}, & \mathcal{O}_8' &= \frac{g_s m_b}{e^2}(\bar{s}\sigma_{\mu\nu}T^a P_L b)G_a^{\mu\nu},\\
\mathcal{O}_9 &= (\bar{s}\gamma_\mu P_L b)(\bar{\ell}\gamma^\mu \ell), & \mathcal{O}_9' &= (\bar{s}\gamma_\mu P_R b)(\bar{\ell}\gamma^\mu \ell),\\
\mathcal{O}_{10} &= (\bar{s}\gamma_\mu P_L b)(\bar{\ell}\gamma^\mu\gamma_5 \ell), & \mathcal{O}_{10}' &= (\bar{s}\gamma_\mu P_R b)(\bar{\ell}\gamma^\mu\gamma_5 \ell),\\
\mathcal{O}_S &= m_b(\bar{s}P_R b)(\bar{\ell}\ell), & \mathcal{O}_S' &= m_b(\bar{s}P_L b)(\bar{\ell}\ell),\\
\mathcal{O}_P &= m_b(\bar{s}P_R b)(\bar{\ell}\gamma_5 \ell), & \mathcal{O}_P' &= m_b(\bar{s}P_L b)(\bar{\ell}\gamma_5 \ell),
\end{aligned}$$

with strength tensor of electromagnetic field $F_{\mu\nu}$ and gluon field $G_{\mu\nu}$, respectively. The new physics effects manifest either in forms of new types of operators and WCs. In SM, only operators $\mathcal{O}_{7,8,9,10}$ turn up while the appearance of their chiral-flipped dual operators with a prime as well as scalar operators $\mathcal{O}_{S,P}^{(\prime)}$ implicate an existence of new physics (NP). As for WCs,

they have been calculated precisely in SM and can be found in [30–33], of which any deviations from their SM results are indications of NP. Especially, NP being embodied in WCs[1] can be denoted as

$$C_{i;\mathrm{NP}}^{(\prime)\ell} \equiv \Delta C_i^{(\prime)\ell} = C_i^{(\prime)\ell} - C_{i;\mathrm{SM}}^{(\prime)\ell}, \tag{3}$$

in which lepton flavors ($\ell = e, \mu$) will be specified in part of following numerical analysis. Although we aim to perform a model-independent analysis, the true NP model is unknown. Thus in following practical analysis, to explore various NP possibilities we discuss different combinations of NP operators as follows.

(I) The muon-specific scenario.
In this case, we set $\Delta C_{9,10,S,P}^{(\prime)\mu}$ and $\Delta C_{7,8}^{(\prime)}$ as free parameters by setting $\Delta C_{9,10,S,P}^{(\prime)e} = 0$.

(II) The lepton-universal scenario.
With $\Delta C_{9,10,S,P}^{(\prime)\mu} = \Delta C_{9,10,S,P}^{(\prime)e}$, the degree of freedoms are $\Delta C_{9,10,S,P}^{(\prime)\mu}$ and $\Delta C_{7,8}^{(\prime)}$.

(III) The lepton-specific scenario.
Here the radiative operators and gluon dipole operators vanish ($\Delta C_7^{(\prime)} = 0, \Delta C_8^{(\prime)} = 0$), while the remaining operators $\Delta C_{9,10,S,P}^{(\prime)\mu;e}$ are unconstrained.

(IV) The full scenario.
In this case, all the parameters $\Delta C_{7,8}^{(\prime)}, \Delta C_{9,10,S,P}^{(\prime)\mu;e}$ are left unrestricted.

The following numerical analysis on the WCs will provide the latest model-independent information. And by making use of the obtained WCs in $b \to s$ FCNC processes, we will discuss some related NP models in a separated paper.

B. Observables in decay processes

We summarize theoretically and experimentally all available decay processes related to $b \to s\ell^+\ell^-$ in this part. As for the choice of experimental data of observables, the adopted data from different collaborations (LHCb, CMS, ATLAS, Belle) will be divided into two datasets. Dataset A contains 201 observables before $R_{K^{(*)}}$ 2022 LHCb release, while dataset B, containing 203 observables, is obtained by replacing LHCb earlier $R_{K^{(*)}}$ results by the 2022 updated one [20].

(I) $B_{s,d} \to \mu^+\mu^-$
The branching fraction of leptonic decay $B_{s,d} \to \mu^+\mu^-$ [30,35] is given as

$$\mathcal{B}(B_{s,d} \to \mu^+\mu^-) = \tau_{B_{s,d}} f_{B_{s,d}}^2 m_{B_{s,d}} \frac{\alpha_e^2 G_F^2}{16\pi^3} |V_{tb} V_{ts(d)}^*|^2 \sqrt{1 - \frac{4m_\mu^2}{m_{B_{s,d}}^2}} \left[|S|^2 \left(1 - \frac{4m_\mu^2}{m_{B_{s,d}}^2}\right) + |P|^2 \right] \tag{4}$$

with

$$S = \frac{m_{B_{s,d}}}{2}(C_S^\mu - C_S^{\mu\prime}),$$
$$P = \frac{m_{B_{s,d}}}{2}(C_P^\mu - C_P^{\mu\prime}) + m_\mu (C_{10}^\mu - C_{10}^{\mu\prime}), \tag{5}$$

in which the SM situation is contained as an extreme example by setting $S \to 0$ and $C_P^{(\prime)} \to 0$ in P. Here the muon flavor in WC has been neglected. For $B_s \to \mu^+\mu^-$, we take into account both the latest LHCb [36] and CMS [37] measured value. So far the branching fraction of $B_d \to \mu^+\mu^-$ has not been measured, we adopt fitting results from different group.

(II) $B \to V\ell^+\ell^-$
Decay modes $B^{+;0} \to K^{*+;0}\mu^+\mu^-$ are both classified into $B \to V\ell\ell$. There are several kinds of observables, including *lepton-universality ratio* (LUR) $R_{K^{(*)}}$, *branching ratios* (BR) [5,11,12,20], *angular distribution observables* (ADO) $P_{1,2,3}$, $P'_{4,5,6,8}$, *forward-backward asymmetry* A_{FB} and *longitude polarization* F_L [5,7,11,14–18,18,19]. The detailed expressions for the observables are given explicitly as

$$\frac{\mathrm{d}\Gamma^\ell}{\mathrm{d}q^2} = \frac{3}{4}\left[2J_{1;s}^\ell\left(C_{7,8,9,10}^{(\prime)\ell}\right) + J_{1;c}^\ell\left(C_{7,8,9,10,S,P}^{(\prime)\ell}\right)\right] - \frac{1}{4}\left[2J_{2;s}^\ell\left(C_{7,8,9,10}^{(\prime)\ell}\right) + J_{2;c}^\ell\left(C_{7,8,9,10}^{(\prime)\ell}\right)\right],$$
$$P_1 \equiv \frac{J_3}{2J_{2;s}}, \qquad P_2 \equiv \frac{-J_{6;s}}{8J_{2;s}}, \qquad P_3 \equiv \frac{J_9}{4J_{2;s}}, \qquad P'_4 \equiv \frac{-J_4}{2\sqrt{-J_{2;s}J_{2:c}}}, \qquad P'_5 \equiv \frac{J_5}{2\sqrt{-J_{2;s}J_{2;c}}},$$

[1]Here we focus on the discussion of CP-conserving NP effects, so these WCs are assumed to be real. The discussion of complex WCs can be referred to [24,34]. C_7' has a little SM contributions proportional to $m_s/m_b C_7$.

$$P_6' \equiv \frac{-J_7}{2\sqrt{-J_{2;s}J_{2;c}}}, \qquad P_8' \equiv \frac{J_8}{2\sqrt{-J_{2;s}J_{2;c}}},$$
$$Q_4 \equiv P_4'^{\mu} - P_4'^{e}, \qquad Q_5 \equiv P_5'^{\mu} - P_5'^{e}, \qquad A_{\rm FB} \equiv \frac{3}{8}(2S_{6;s} + S_{6;c}), \qquad F_{\rm L} \equiv -S_{2;c}, \tag{6}$$

among which $C_{S,P}^{(\prime)}$ only involved in Γ^{ℓ}, P_5', and $A_{\rm FB}$. The definitions of J_i and S_i can be referred to Appendix (A 2). As for $B^0 \to K^{*0}e^+e^-$ mode, 4 angular observables measured by LHCb [38] are also included in this analysis.

(III) $B \to P\ell^+\ell^-$

Two modes $B^{+;0} \to K^{+;0}\mu^+\mu^-$ have been measured in this class involving pseudoscalar meson final states, offering LUR [6,9–11,20] and BR [6,9,11,13] as observables. Branching fractions can be calculated as

$$\frac{d\Gamma^{\ell}}{dq^2} = |V_{tb}V_{ts}^*|^2 \frac{G_F^2\alpha_e^2 M_B^3}{256\pi^5}\lambda\xi_P^2 \left[I_a^{\ell}\left(q^2; C_{7,8,9,10,S,P}^{(\prime)}\right) + \frac{1}{3} I_c^{\ell}\left(q^2; C_{7,8,9,10}^{(\prime)}\right)\right], \tag{7}$$

and more details can be found in Appendix (A 3).

(IV) $B_s \to \phi\mu^+\mu^-$

Theoretical formula for branching fraction are similar to $B \to V\ell^+\ell^-$ Eq. (6), up to form factors (FFs) and spectator effects. LHCb measurement of BR and F_L [39,40] are taken as experimental inputs in the numerical calculations.

(V) $B \to X_s\ell^+\ell^-$

The inclusive process provides complementary information to those exclusive modes. Here we follow the conventions in [41–43] and the differential branching fraction[2] can be written as,

$$\frac{d\mathcal{B}(B \to X_s\ell^+\ell^-)}{d\hat{s}} = \frac{\mathcal{B}(B \to X_c\ell\bar{\nu})\alpha_e^2}{4\pi^2 f(z)\kappa(z)} \frac{|V_{tb}V_{ts}^*|^2}{|V_{cb}|^2}(1-\hat{s})^2 \times \sqrt{1 - \frac{4\hat{m}_{\ell}}{\hat{s}}}\tilde{N}\left(\hat{s}; \hat{m}_{\ell}; C_{7,8,9,S,P}^{(\prime)}\right), \tag{8}$$

where the definitions of $f(z)$ and $\kappa(z)$ can be found in [43]. The latest theoretical formulas incorporating high-order corrections can be found in [44,45]. As a part of inputs, the experimental data is taken from *BABAR* 2014 measurement [46].

(VI) Radiative decays: $B \to X_s\gamma$, $B \to K^0\gamma$, $B^+ \to K^{*+}\gamma$, $B \to \phi\gamma$

This class of decays, related to $b \to s\gamma$, give stringent constraint on penguin box diagram and hence $\Delta C_7^{(\prime)}$. For the inclusive radiative decay $B \to X_s\gamma$, we follow [41,47,48] by using matrices $K_{ij}^{(1,2)}$ from *flavio* [49] related to $P(E_0)$ as well as formula C from [50],

$$\mathcal{B}(\bar{B} \to X_s\gamma) = \mathcal{B}(\bar{B} \to X_c e\bar{\nu})_{\rm exp}\left|\frac{V_{ts}^*V_{tb}}{V_{cb}}\right|^2 \times \frac{6\alpha_e}{\pi C}[P(E_0; C_{7,8}) + N(E_0; C_{7,8}) + \epsilon_{\rm EM}(C_{7,8})], \tag{9}$$

where the $N(E_0; C_{7,8})$ represents nonperturbative correction as well as $\epsilon_{\rm EM}(C_{7,8})$ is the electromagnetic correction. Both of their formulas can be found in [41]. As for $B \to V\gamma$ process, the simplified formula [51] is adopted,

$$\mathcal{B}(B_q \to V\gamma) = \tau_{B_q}\frac{\alpha_e G_F^2 m_{B_q}^3 m_b^2}{32\pi^4}\left(1 - \frac{m_V^2}{m_B^2}\right)^3 \times |\lambda_t|^2(|C_7^{\rm eff}|^2 + |C_7'^{\rm eff}|^2)T_1(0), \tag{10}$$

where $T_1(q^2 = 0)$ can be found in Table II. Especially, 3 observable $S_{\phi\gamma}, A_{\rm CP}, A_{\Delta\Gamma}$ in $B \to \phi\gamma$ process are also incorporated. Their expressions can be found in [52]. The experimental[3] inclusive results are taken from Belle 2014 [53] while the exclusive ones are originated from Belle (2014 and 2021) as well as LHCb 2019 [54–56] measurements.

(VII) $\Lambda_b \to \Lambda\mu^+\mu^-$

As the $b \to s\ell\ell$ related bottomed baryon decay, $\Lambda_b \to \Lambda\mu^+\mu^-$, shares some common features with $B \to V\ell\ell$. In low-q^2 bins, deviations from SM predictions have been found. Following [57,58], the differential width as well as involved FFs is given as

$$\frac{d\Gamma^{\ell}}{dq^2} \equiv 2J_{1ss}^{\ell}(C_{7,9,10}^{(\prime)}) + J_{1cc}^{\ell}(C_{7,9,10}^{(\prime)}). \tag{11}$$

More details can be referred to Appendix A 5. For the experimental observed branching fraction, we refer to the LHCb 2015 measurement [59].

[2]Note that their $C_{Q_1;Q_2}$ are related to our definition $C_{Q_1;Q_2} = m_b C_{S;P}$, so we re-scale their WCs with MS mass $\bar{m}_b$.

[3]A cut on photon energy E_0 is extrapolated from 1.9 GeV to 1.6 GeV in practice.

In both cases before and after $R_{K^{(*)}}$ 2022 release, there are more than 200 observables related to the above processes, including the binned ones. A detailed summary of experimental data of these observables are listed in Appendix B.

C. Fitting schemes

In our following fitting work, Bayesian statistics is adopted, based on which some early analysis on B-anomalies [60–63] is also performed. The advantages of carrying out a Bayesian estimation are its robustness and extensibility. For robustness, firstly, Bayesian inference with posterior functions has the advantage of avoiding the danger of insufficient coverage probability compared to the traditional *profile* method that used to derive confidence intervals. Second, more attention can be paid to the distribution of parameters, namely overall effects, rather than to an individual minimum.

We denote the posterior function according to Bayesian theorem,

$$\mathcal{P}(\vec{\theta}|\mathcal{O}_{\text{expt}}) \propto \mathcal{L}(\mathcal{O}|\vec{\theta})\pi(\vec{\theta}), \tag{12}$$

where $\mathcal{L}(\mathcal{O}|\vec{\theta})$ and $\pi(\vec{\theta})$ stand for the likelihood function and prior we set, respectively. In our model-independent fit, a negative log likelihood (NLL) function is defined as

$$\begin{aligned} -2\log\mathcal{L}(\mathcal{O}|\vec{\theta}) &= \chi^2(\vec{\theta}) \\ &= (\mathcal{O}_{\text{theo}}(\vec{\theta}) - \mathcal{O}_{\text{expt.}})^{\top}(V_{\text{expt}} + V_{\text{theo}})^{-1} \\ &\quad \times (\mathcal{O}_{\text{theo}}(\vec{\theta}) - \mathcal{O}_{\text{expt}}), \end{aligned} \tag{13}$$

where $\mathcal{O}_{\text{theo}}$ as well as $\mathcal{O}_{\text{expt}}$ represent the theoretical predictions of various observables and their corresponding experimental data. The covariance matrices V_{theo} and V_{expt} are consist of theoretical and experimental errors of observables. For the experimental correlation matrix, we have taken into account some of the correlations among relevant experiments [16,17,20,36–38,56], while the error is aligned to the bigger one in the asymmetrical error case. Theoretical covariance matrix is formed by assuming a multivariate Gaussian distribution of input parameters which would mainly occupy the pie chart of error (form factors error for example). Both matrices are N dimensional, where N is the number of observables up to 203. The parameter matrix $\vec{\theta}$ shown above, is encoded various WCs,

$$\begin{aligned} \vec{\theta} = (&\Delta C_7, \Delta C_7', \Delta C_8, \Delta C_8', \Delta C_9^{\ell}, \Delta C_9'^{\ell}, \Delta C_{10}^{\ell}, \\ &\times \Delta C_{10}'^{\ell}, \Delta C_S^{\ell}, \Delta C_S'^{\ell}, \Delta C_P^{\ell}, \Delta C_P'^{\ell}), \end{aligned} \tag{14}$$

where $\ell = e$ or μ, and the dimension can be as large as 20 in some of the working scenarios.

The likelihood function tells us where we are heading, while the prior distribution $\pi(\vec{\theta})$ tells us where to start. The prior function usually implies the extent of our knowledge about the problem we are facing. Namely, in these fits, it represents the more probable starting position (or the coordinate of WCs) as well as their ranges. In our analysis, the best-fit point obtained from HMMN [25] is taken as our prior knowledge. So a prior of multidimensional Gaussian distribution which is centered at the latest 20-D fit result from HMMN [25] with a common standard deviation of $\sqrt{2}$ is utilized.

III. NUMERICAL ANALYSIS

A. Input parameters

The global fitting analysis, relying on χ^2 function, contains both theoretical and experimental inputs. In Appendix A, we present the necessary theoretical formulas for various observables in related decay processes. For the WCs, we adopted the obtained results from [33], which have been calculated at μ_b scale with two-loop RGE running. Other basic parameters (masses, lifetimes, Wolfenstein parameters in CKM matrix, decay constants, Weinberg angles, etc.) and some nonperturbative parameters (Gegenbaur expansion coefficients in distribution amplitudes (DA), FFs, etc.) have been summarized in Table I and II, respectively. As another part of inputs, the experimental data of various observables shown bin by bin, have been presented in Appendix B, together with their corresponding calculated SM predictions.

In order to depict the goodness of fit of different scenarios, we adopt a method that is often utilized by frequentists: performing a reduced chi-squared $\chi^2/\text{d.o.f.}$. We first make a histogram of samples from the negative log-likelihood (NLL) distribution. The numerator of the reduced chi-squared is then the χ^2 corresponding to the maximum density of the NLL distribution. This is in contrast to the traditional frequentist approach, which only considers the minimum chi-squared.

To estimate the parameters $\vec{\theta}$, we adopt the median as our estimation of the center value of the parameter for its robustness. We then use the 16th and 84th percentiles to indicate the boundary of our one standard deviation confidence interval. This region has the same coverage probability as the standard normal distribution.

B. Numerical results

To interpret the 2022 release of $R_{K^{(*)}}$ in a global picture of $b \to s\ell^+\ell^-$, we carry out global fits in four aforementioned scenarios based on two different datasets, dataset A and B. We use Figs. 1 and 2 to illustrate the central values and errors of typical parameters, ΔC_9^{μ} and ΔC_{10}^{μ}, with Bayesian statistics. The first row of figures in Figs. 1 and 2 are produced based on the early dataset A, while the second row corresponds to dataset B. The central values of the

TABLE I. Input parameters I: some basic parameters in the numerical analysis.

Parameters	Values	Parameters	Values
m_b	$4.18(^{+3}_{-2})$ GeV [64]	m_t	173.50(30) GeV [64]
m_c	1.27(2) GeV [64]	m_s	$93(^{+11}_{-5})$ MeV [64]
m_d	$4.67(^{+48}_{-17})$ MeV [64]	m_u	$2.16(^{+49}_{-26})$ MeV [64]
m_e	0.5109989461(31) MeV [64]	m_μ	105.6583745(24) MeV [64]
m_τ	1776.86(12) MeV [64]	m_{B_s}	5366.92(10) MeV [64]
m_{B_d}	5279.65(12) MeV [64]	m_ϕ	1019.461(16) MeV [64]
$m_{K^\pm}$	493.677(16) MeV [64]	m_{K^0}	497.611(13) MeV [64]
$m_{K^{*\pm}}$	891.67(26) MeV [64]	$m_{K^{*0}}$	895.55(20) MeV [64]
m_{B_u}	5279.34(12) MeV [64]	m_Λ	1115.683(6) MeV [64]
m_{Λ_b}	5619.60(17) MeV [64]	τ_{B_u}	1.638(4) ps [64]
τ_{B_s}	1.520(5) ps [64]	τ_{B_d}	1.519(4) ps [64]
τ_{Λ_b}	1.471(9) ps [64]		
f_{B_s}	227.7(4.5) MeV [65]	f_{B_d}	190.5(4.2) MeV [65]
f_Λ	$6.0(4) \times 10^{-3}$ GeV^2 [66]	f_{Λ_b}	$3.9(^{+4}_{-2}) \times 10^{-3}$ GeV^2 [66]
$m_t(m_t)$	163.53(83) GeV [64]	G_F	$1.1663787(6) \times 10^{-5}$ GeV^{-2} [64]
α_Λ	0.642(13) [58]	$\alpha_e(m_Z)$	1/127.944(14) [65]
$\alpha_s(m_Z)$	0.1179(9) [64]	$\sin^2\theta_W$	0.23121(4) [64]
y_s	0.064(4) [64]	y_d	0.0005(50) [64]
μ_G^2	0.336(64) [50]		
ρ_D^3	0.153(45) [50]	ρ_{LS}^3	−0.145(98) [50]
$\mathcal{B}(B \to X_c e\bar{\nu})_{\rm exp}$	0.0997(41) [67]	$\mathcal{B}(B \to X_c \ell\bar{\nu})_{\rm exp}$	0.0975(50) [67]
λ	0.22500(67) [64]	A	$0.826(^{+18}_{-15})$ [64]
$\bar{\rho}$	$0.159(^{+10}_{-10})$ [64]	$\bar{\eta}$	$0.348(^{+10}_{-10})$ [64]

parameters, mainly located at around well-known −1 and 0.2, differ slightly from scenarios in both two sets of fits. On the other hand, to understand how the global change occurs due to the 2022 update of $R_{K^{(*)}}$, a comparison between the results of the two datasets is necessary. Taking ΔC_9^μ shown in Fig. 1 as an example, the central values in all the scenarios vary, but not dramatically, while the errors almost keep unchanged.

Incorporating all the WCs analyzed in various scenarios based on both dataset A and B. We summarize the results of all the fitted parameters characterizing new physics effects in Tables III and IV, respectively. The numbers of fitted parameters in our analysis are two sets of 12, one set of 16, and 20, denoted as scenario I, II, III, and IV (S-I, S-II, S-III, and S-IV, or those corresponding ones with a prime). As a comparison, early global fits made by other four independent analyses [23–26] (one group of 20-D, one group of 6-D, and two groups of 4-D parameters) are also listed in the two tables.

To confirm the correctness of our numerical calculation, we first perform a calculation based on dataset A, as shown in Table III, in different working scenarios (with a prime). Our fitted WCs of muon flavor are consistent not only with each scenario but also with the other four independent groups within the fitted errors. WCs involving electron flavor have been studied less, and early efforts can be found in the two groups AS [24] and HMMN [25]. With similar errors (1.2 and 1.9) but obvious different central values (−0.24 and −6.50) for ΔC_9^e, it is not easy to judge how its deviation from the SM prediction. Our calculations in both S-III' (-1.8 ± 0.8) and S-IV' (-1.6 ± 0.6) provide self-consistent information and support a negative deviation from the SM about 2.5σ. As for ΔC_{10}^e, it can be concluded that the deviation from the SM is within 1σ, combining all our calculations (S-II', III', and IV') as well as the work done by AS [24] and HMMN [25]. In general, the errors of scalar operator WCs in HMMN [25] are smaller than ours. Though we both make a consistent description (less than 2σ deviation) for $\Delta C_{S,P}^{(\prime)\mu}$ and $\Delta C_S^{(\prime)e}$, the feature of $\Delta C_P^{(\prime)e}$ differs. Our calculation prefers a SM-like behavior while HMMN [25] suggests a deviation of around 4σ, requiring further clarification by incorporating more and more precise data as well as more efforts on fitting.

The impact of the 2022 $R_{K^{(*)}}$ data is detailed in Table IV. The new physics potential in ΔC_9^μ, which was highly anticipated before, has been widely questioned since the release of $R_{K^{(*)}}^{2022}$. According to the numerical results in Table IV, the roughly 4σ standard deviations still exist in each scenario, with slight shifts in central values and almost unchanged errors. The SM-like behavior of $\Delta C_{7,8}^{(\prime)}$, within a 2σ deviation, remains unchanged from the earlier data.

TABLE II. Form factors as well as resonance pole mass used in the numerical analysis of $B \to P\ell^+\ell^-$ [68], $B \to V\ell^+\ell^-$ [69], $B \to V\gamma$ [51] and $\Lambda_b \to \Lambda\ell^+\ell^-$ [58], respectively.

Parameters	Values	Parameters	Values
$f_+(0)$	$0.34^{+0.05}_{-0.02}$	a_+^1	$-2.1^{+0.9}_{-1.6}$
$m_{\mathrm{res},+}$	5.412 GeV		
$a_0^{A_0}(K^*)$	$+0.36 \pm 0.05$	$a_0^{A_0}(\phi)$	$+0.39 \pm 0.05$
$a_1^{A_0}(K^*)$	-1.04 ± 0.27	$a_1^{A_0}(\phi)$	-0.78 ± 0.26
$a_2^{A_0}(K^*)$	$+1.12 \pm 1.35$	$a_2^{A_0}(\phi)$	$+2.41 \pm 1.48$
$a_0^{T_1}(K^*)$	$+0.28 \pm 0.03$	$a_0^{T_1}(\phi)$	$+0.31 \pm 0.03$
$a_1^{T_1}(K^*)$	-0.89 ± 0.19	$a_1^{T_1}(\phi)$	-0.87 ± 0.19
$a_2^{T_1}(K^*)$	$+1.95 \pm 1.10$	$a_2^{T_1}(\phi)$	$+2.75 \pm 1.19$
$m_{\mathrm{res},A_0}(K^*)$	5.366 GeV	$m_{\mathrm{res},A_0}(\phi)$	5.366 GeV
$m_{\mathrm{res},T_1}(K^*)$	5.415 GeV	$m_{\mathrm{res},T_1}(\phi)$	5.415 GeV
$T_1^{\phi}(0)$	$0.280^{+0.020}_{-0.022}$	$T_1^{K^*}(0)$	$0.316^{+0.016}_{-0.015}$
$a_0^{f_+}$	$+0.4221 \pm 0.0188$	$a_1^{g_0}$	-1.0290 ± 0.1614
$a_1^{f_+}$	-1.1386 ± 0.1683	$a_1^{g_\perp}$	-1.1357 ± 0.1911
$a_0^{f_0}$	$+0.3725 \pm 0.0213$	$a_0^{h_+}$	$+0.4960 \pm 0.0258$
$a_1^{f_0}$	-0.9389 ± 0.2250	$a_1^{h_+}$	-1.1275 ± 0.2537
$a_0^{f_\perp}$	$+0.5182 \pm 0.0251$	$a_0^{h_\perp}$	$+0.3876 \pm 0.0172$
$a_1^{f_\perp}$	-1.3495 ± 0.2413	$a_1^{h_\perp}$	-0.9623 ± 0.1550
$a_0^{g_\perp, g_+}$	0.3563 ± 0.0142	$a_0^{\tilde{h}_\perp, \tilde{h}_+}$	$+0.3403 \pm 0.0133$
$a_1^{g_+}$	-1.0612 ± 0.1678	$a_1^{\tilde{h}_+}$	-0.7697 ± 0.1612
$a_0^{g_0}$	0.4028 ± 0.0182	$a_1^{\tilde{h}_\perp}$	-0.8008 ± 0.1537
$m_{\mathrm{res},(f_+;f_\perp;h_+;h_\perp)}$	5.416 GeV	$m_{\mathrm{res},(g_+;g_\perp;\tilde{h}_+;\tilde{h}_\perp)}$	5.750 GeV
$m_{\mathrm{res},(f_0)}$	5.711 GeV	$m_{\mathrm{res},(g_0)}$	5.367 GeV

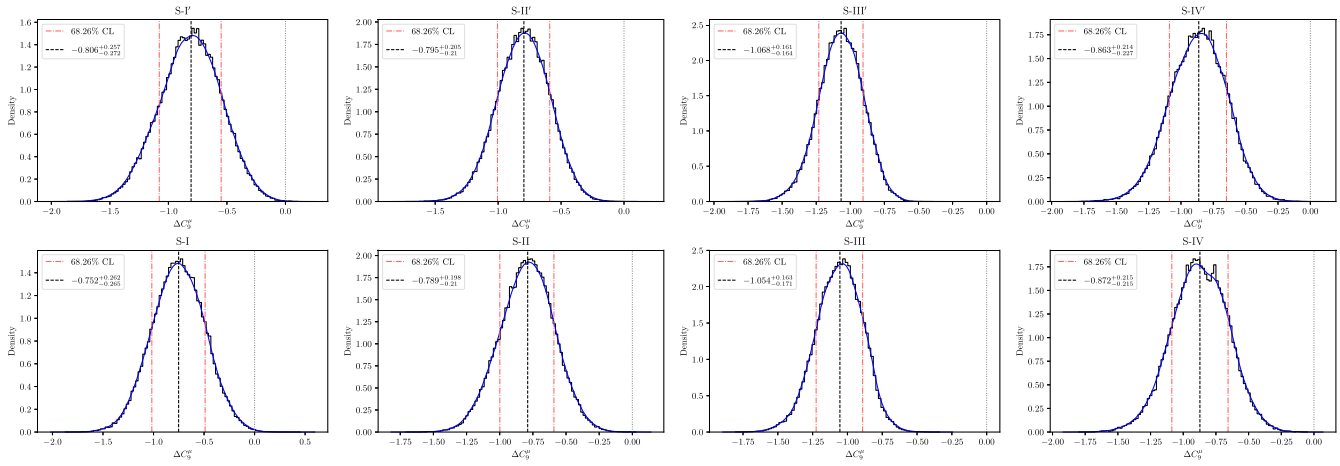

FIG. 1. Density (black steps) and kernel density estimation KDE (blue curves) of Wilson coefficients ΔC_9^μ in different scenarios varied from old dataset A to B. Red (dotdashed) lines indicate the highest posterior density (HPD) about 68.26% which give the error estimations. Black (dashed) lines refer to the Bayesian estimations of ΔC_9^μ while gray(dotted) lines refer to SM positions.

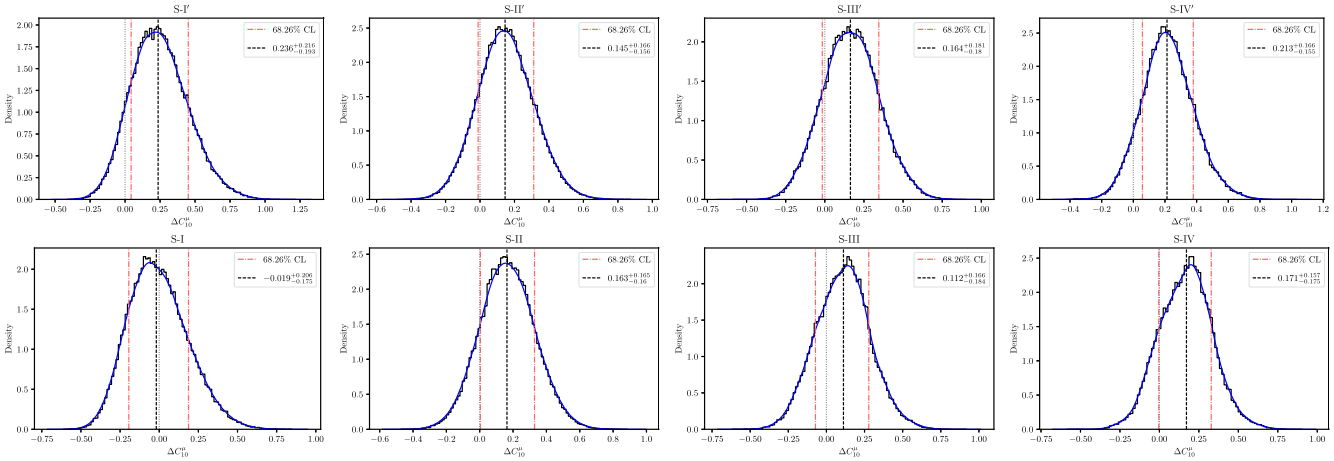

FIG. 2. Density (black steps) and KDE (blue curves) of Wilson coefficients ΔC_{10}^{μ} in different scenarios varied from old dataset A to B. Intervals between the two red (dotdashed) lines cover the HPD about 68.26% to estimate 1σ range. The remaining indicators black (dashed) and gray (dotted) lines play a similar role as the description of Fig. 1.

The situation for other muon flavor related fitted parameters depends on the number of fitting parameters. For example, the fitted ΔC_9^{μ} in S-III exhibits a decreased standard deviation from 6.6σ in dataset A to 6.4σ in dataset B. Therefore, it can be safely said that all the muon type WCs except ΔC_9^{μ} are all within 2σ deviations. Moreover, the updated ΔC_9^{e} values are consistent with the previous values shown in Table III. The deviation in Scenario III still keeps

TABLE III. Global fits in various scenarios based on dataset A with $\chi^2_{\rm SM} = 287.424$ which calculated by setting all WCs to be zero as well as corresponding observables $n = 201$.

Params	S-I'	S-II'	S-III'	S-IV'	ACDMN [23]	AS [24]	HMMN [25]	GGJLCS [26]
Reduced χ^2	183.404/(n-12)	197.556/(n-12)	182.869/(n-16)	176.807/(n-20)	260.66/(254-6)		179.1/(183-20)	96.88/90
$\chi^2_{\rm min}$/d.o.f	= 0.970	= 1.045	= 0.988	= 0.977	= 1.05		= 1.1	= 1.08
ΔC_7	$-0.003^{+0.020}_{-0.019}$	$-0.001^{+0.015}_{-0.015}$	⋯	$0.001^{+0.016}_{-0.015}$	$0.00^{+0.01}_{-0.02}$	⋯	$0.06^{-0.03}_{+0.03}$	⋯
$\Delta C_7'$	$0.017^{+0.018}_{-0.019}$	$0.020^{+0.014}_{-0.015}$	⋯	$0.020^{+0.014}_{-0.014}$	$+0.00^{+0.02}_{-0.01}$	⋯	$-0.01^{-0.01}_{+0.01}$	⋯
ΔC_8	$-0.788^{+0.595}_{-0.514}$	$-0.885^{+0.435}_{-0.398}$	⋯	$-0.773^{+0.451}_{-0.449}$	⋯	⋯	$-0.80^{-0.40}_{+0.40}$	⋯
$\Delta C_8'$	$-0.073^{+1.089}_{-1.000}$	$-0.093^{+0.921}_{-0.831}$	⋯	$-0.089^{+0.996}_{-0.922}$	⋯	⋯	$-0.30^{+1.30}_{-1.30}$	⋯
ΔC_9^{μ}	$-0.806^{+0.257}_{-0.272}$	$-0.795^{+0.205}_{-0.210}$	$-1.068^{+0.161}_{-0.164}$	$-0.863^{+0.214}_{-0.227}$	$-1.08^{+0.18}_{-0.17}$	$-0.82^{+0.23}_{-0.23}$	$-1.14^{-0.19}_{+0.19}$	$-1.07^{+0.29}_{-0.29}$
$\Delta C_9'^{\mu}$	$0.194^{+0.395}_{-0.416}$	$0.056^{+0.338}_{-0.342}$	$0.112^{+0.393}_{-0.397}$	$0.020^{+0.346}_{-0.362}$	$0.16^{+0.37}_{-0.36}$	$-0.10^{+0.34}_{-0.34}$	$0.05^{+0.32}_{-0.32}$	$0.32^{-0.21}_{+0.21}$
ΔC_{10}^{μ}	$0.236^{+0.216}_{-0.193}$	$0.145^{+0.166}_{-0.156}$	$0.164^{+0.181}_{-0.180}$	$0.213^{+0.166}_{-0.155}$	$0.15^{+0.13}_{-0.13}$	$+0.14^{+0.23}_{-0.23}$	$0.21^{-0.20}_{+0.20}$	$0.21^{-0.14}_{+0.14}$
$\Delta C_{10}'^{\mu}$	$-0.096^{+0.251}_{-0.237}$	$-0.108^{+0.186}_{-0.177}$	$-0.115^{+0.200}_{-0.198}$	$-0.089^{+0.177}_{-0.176}$	$-0.18^{+0.20}_{-0.18}$	$-0.33^{+0.23}_{-0.23}$	$-0.03^{+0.19}_{-0.19}$	$-0.26^{-0.14}_{+0.14}$
ΔC_S^{μ}	$0.066^{+1.091}_{-1.142}$	$-0.004^{+1.102}_{-1.131}$	$-0.008^{+0.883}_{-0.899}$	$-0.043^{+0.842}_{-0.875}$	⋯	⋯	$0.01^{+0.05}_{-0.05}$	⋯
$\Delta C_S'^{\mu}$	$0.065^{+1.087}_{-1.140}$	$0.003^{+1.103}_{-1.126}$	$-0.002^{+0.873}_{-0.936}$	$-0.059^{+0.844}_{-0.869}$	⋯	⋯	$-0.01^{+0.05}_{-0.05}$	⋯
ΔC_P^{μ}	$0.167^{+1.172}_{-1.225}$	$1.017^{+0.735}_{-0.816}$	$0.092^{+1.076}_{-0.994}$	$0.117^{+0.847}_{-0.894}$	⋯	⋯	$-0.04^{+0.02}_{-0.02}$	⋯
$\Delta C_P'^{\mu}$	$0.053^{+1.169}_{-1.227}$	$0.891^{+0.729}_{-0.812}$	$0.010^{+1.083}_{-1.002}$	$0.040^{+0.854}_{-0.895}$	⋯	⋯	$-0.04^{+0.02}_{-0.02}$	⋯
ΔC_9^{e}	⋯	$-0.795^{+0.205}_{-0.210}$	$-1.753^{+0.781}_{-0.772}$	$-1.551^{+0.627}_{-0.599}$	⋯	$-0.24^{+1.17}_{-1.17}$	$-6.50^{+1.90}_{-1.90}$	⋯
$\Delta C_9'^{e}$	⋯	$0.056^{+0.338}_{-0.342}$	$1.725^{+1.724}_{-2.286}$	$1.710^{+1.466}_{-1.764}$	⋯	⋯	$1.40^{+2.30}_{-2.30}$	⋯
ΔC_{10}^{e}	⋯	$0.145^{+0.166}_{-0.156}$	$0.108^{+1.456}_{-0.661}$	$0.058^{+1.193}_{-0.661}$	⋯	$-0.24^{+0.78}_{-0.78}$	∼0	⋯
$\Delta C_{10}'^{e}$	⋯	$-0.108^{+0.186}_{-0.177}$	$0.600^{+1.208}_{-1.099}$	$0.655^{+0.958}_{-0.841}$	⋯	⋯	∼0	⋯
ΔC_S^{e}	⋯	$-0.004^{+1.102}_{-1.131}$	$-0.719^{+1.861}_{-1.227}$	$-0.549^{+1.602}_{-1.232}$	⋯	⋯	$-0.38^{+0.41}_{-0.41}$	⋯
$\Delta C_S'^{e}$	⋯	$0.003^{+1.103}_{-1.126}$	$-0.699^{+1.837}_{-1.224}$	$-0.550^{+1.618}_{-1.326}$	⋯	⋯	$-0.36^{+0.50}_{-0.50}$	⋯
ΔC_P^{e}	⋯	$1.017^{+0.735}_{-0.816}$	$-1.592^{+1.552}_{-1.079}$	$-1.688^{+1.366}_{-0.978}$	⋯	⋯	$-0.98^{+0.21}_{-0.21}$	⋯
$\Delta C_P'^{e}$	⋯	$0.891^{+0.729}_{-0.812}$	$-1.360^{+1.318}_{-1.149}$	$-1.431^{+1.212}_{-1.017}$	⋯	⋯	$-0.95^{+0.29}_{-0.29}$	⋯

TABLE IV. Global fits in various scenarios based on dataset B with $\chi^2_{\rm SM} = 265.888$ originated from $\Delta C_i = 0$ and the number of observables $n = 203$.

Params	S-I	S-II	S-III	S-IV	ADCMN [23]	AS [24]	HMMN [25]	GGJLCS [26]
Reduced χ^2	190.044/(n-12)	177.891/(n-12)	185.386/(n-16)	178.953/(n-20)	260.66/(254-6)		179.1/(183-20)	96.88/90
$\chi^2_{\rm min}$/d.o.f	= 0.995	= 0.931	= 0.991	= 0.978	= 1.05		= 1.1	= 1.08
ΔC_7	$-0.000^{+0.020}_{-0.020}$	$-0.001^{+0.015}_{-0.015}$	⋯	$-0.000^{+0.016}_{-0.015}$	$0.00^{+0.01}_{-0.02}$	⋯	$0.06^{-0.03}_{+0.03}$	⋯
$\Delta C'_7$	$0.017^{+0.020}_{-0.018}$	$0.020^{+0.015}_{-0.014}$	⋯	$0.023^{+0.014}_{-0.016}$	$+0.00^{+0.02}_{-0.01}$	⋯	$-0.01^{-0.01}_{+0.01}$	⋯
ΔC_8	$-0.995^{+0.540}_{-0.463}$	$-0.921^{+0.443}_{-0.378}$	⋯	$-0.773^{+0.465}_{-0.424}$	⋯	⋯	$-0.80^{-0.40}_{+0.40}$	⋯
$\Delta C'_8$	$-0.080^{+1.046}_{-0.942}$	$-0.076^{+0.893}_{-0.833}$	⋯	$-0.258^{+1.007}_{-0.802}$	⋯	⋯	$-0.30^{+1.30}_{-1.30}$	⋯
ΔC_9^μ	$-0.752^{+0.262}_{-0.265}$	$-0.789^{+0.198}_{-0.210}$	$-1.054^{+0.163}_{-0.171}$	$-0.872^{+0.215}_{-0.215}$	$-1.08^{+0.18}_{-0.17}$	$-0.82^{+0.23}_{-0.23}$	$-1.14^{-0.19}_{+0.19}$	$-1.07^{+0.29}_{-0.29}$
$\Delta C_9^{\prime\mu}$	$0.174^{+0.434}_{-0.441}$	$0.048^{+0.338}_{-0.348}$	$0.130^{+0.439}_{-0.437}$	$0.088^{+0.342}_{-0.378}$	$0.16^{+0.37}_{-0.36}$	$-0.10^{+0.34}_{-0.34}$	$0.05^{+0.32}_{-0.32}$	$0.32^{-0.21}_{+0.21}$
ΔC_{10}^μ	$-0.019^{+0.206}_{-0.175}$	$0.163^{+0.165}_{-0.160}$	$0.112^{+0.166}_{-0.184}$	$0.171^{+0.157}_{-0.175}$	$0.15^{+0.13}_{-0.13}$	$+0.14^{+0.23}_{-0.23}$	$0.21^{-0.20}_{+0.20}$	$0.21^{-0.14}_{+0.14}$
$\Delta C_{10}^{\prime\mu}$	$-0.118^{+0.266}_{-0.247}$	$-0.093^{+0.183}_{-0.179}$	$-0.115^{+0.215}_{-0.213}$	$-0.062^{+0.197}_{-0.180}$	$-0.18^{+0.20}_{-0.18}$	$-0.33^{+0.23}_{-0.23}$	$-0.03^{+0.19}_{-0.19}$	$-0.26^{-0.14}_{+0.14}$
ΔC_S^μ	$0.023^{+1.064}_{-1.097}$	$0.060^{+1.188}_{-1.230}$	$-0.066^{+0.944}_{-0.929}$	$0.009^{+0.858}_{-0.845}$	⋯	⋯	$0.01^{+0.05}_{-0.05}$	⋯
$\Delta C_S^{\prime\mu}$	$0.014^{+1.064}_{-1.086}$	$0.061^{+1.188}_{-1.225}$	$-0.070^{+0.957}_{-0.930}$	$0.012^{+0.858}_{-0.862}$	⋯	⋯	$-0.01^{+0.05}_{-0.05}$	⋯
ΔC_P^μ	$0.079^{+1.159}_{-1.146}$	$0.478^{+0.808}_{-0.899}$	$0.189^{+1.018}_{-1.028}$	$0.124^{+0.902}_{-0.910}$	⋯	⋯	$-0.04^{+0.02}_{-0.02}$	⋯
$\Delta C_P^{\prime\mu}$	$-0.032^{+1.158}_{-1.145}$	$0.370^{+0.803}_{-0.897}$	$0.098^{+1.009}_{-1.024}$	$0.038^{+0.894}_{-0.913}$	⋯	⋯	$-0.04^{+0.02}_{-0.02}$	⋯
ΔC_9^e	⋯	$-0.789^{+0.198}_{-0.210}$	$-1.623^{+0.662}_{-0.734}$	$-1.511^{+0.561}_{-0.533}$	⋯	$-0.24^{+1.17}_{-1.17}$	$-6.50^{+1.90}_{-1.90}$	⋯
$\Delta C_9^{\prime e}$	⋯	$0.048^{+0.338}_{-0.348}$	$1.090^{+1.610}_{-1.793}$	$0.864^{+1.483}_{-1.608}$	⋯	⋯	$1.40^{+2.30}_{-2.30}$	⋯
ΔC_{10}^e	⋯	$0.163^{+0.165}_{-0.160}$	$0.555^{+1.042}_{-0.576}$	$0.383^{+0.840}_{-0.424}$	⋯	$-0.24^{+0.78}_{-0.78}$	∼0	⋯
$\Delta C_{10}^{\prime e}$	⋯	$-0.093^{+0.183}_{-0.179}$	$0.088^{+0.969}_{-0.956}$	$0.002^{+0.881}_{-0.815}$	⋯	⋯	∼0	⋯
ΔC_S^e	⋯	$0.060^{+1.188}_{-1.230}$	$-0.952^{+2.122}_{-1.139}$	$-0.806^{+1.900}_{-1.238}$	⋯	⋯	$-0.38^{+0.41}_{-0.41}$	⋯
$\Delta C_S^{\prime e}$	⋯	$0.061^{+1.188}_{-1.225}$	$-1.051^{+2.251}_{-1.075}$	$-0.803^{+1.861}_{-1.194}$	⋯	⋯	$-0.36^{+0.50}_{-0.50}$	⋯
ΔC_P^e	⋯	$0.478^{+0.808}_{-0.899}$	$-1.568^{+1.544}_{-1.149}$	$-1.837^{+1.376}_{-0.930}$	⋯	⋯	$-0.98^{+0.21}_{-0.21}$	⋯
$\Delta C_P^{\prime e}$	⋯	$0.370^{+0.803}_{-0.897}$	$-1.477^{+1.409}_{-1.083}$	$-1.652^{+1.200}_{-0.979}$	⋯	⋯	$-0.95^{+0.29}_{-0.29}$	⋯

around 2.3σ, with both slight decreased central value and error. The deviation in Scenario IV shifts from 2.6σ to 2.8σ. All other electron type WCs, including $\Delta C^{(\prime)e}_{10,S,P}$, are found to be restricted within around 1σ.

In addition to the 1-D parameter projections from the high dimensional full parameter space shown in Tables III and IV, more information can be drawn from correlations among 2-D parameters. In many previous studies, lepton flavors in $\mathcal{O}^{(\prime)}_{9,10}$ as well as $\mathcal{O}^{(\prime)}_{S,P}$ are usually not discriminated. This assumption is also adopted as one of our working scenarios (S-II or S-II'). However, it is important to keep in mind that relaxing the identical lepton flavor restriction is also possible. We present explicitly in Fig. 3, the correlations between WCs of the same type among by specifying the lepton flavors in Scenario III and IV based on dataset B. The locations of the best fit points and the 1σ allowed regions are dependent on the working scenario, as shown by the analysis of left-handed operators in Fig. 3. A straight line passing through the origin with a slope of 1 represents lepton flavor independence. In almost all of the two scenarios (S-III and S-IV), ΔC_9 and $\Delta C_{S,P}$ deviate from this line in the 1σ region, while ΔC_{10} contains part of the "flavor identical line" in its 1σ region. But in 2σ regions, the flavor identical line can be contained by all $\Delta C_{9,10}$ and $\Delta C_{S,P}$. Therefore, at the 1σ level, the identical lepton flavor is only respected by ΔC_{10} but can be extended to all at the 2σ level.

The relations between operators with opposite chirality are also of interest. We show them in the form of 2-D correlations in Fig. 4. Similar to the flavor situation, we take the line with slope of 1 and intercept of 0 as a criterion to judge the chirality dependence from data. Apparently, the deviations of such a line, at the 2σ level, in all the four scenarios of ΔC_9^μ indicate that ΔC_9^μ and $\Delta C_9^{\prime\mu}$ are indeed two separated parameters. As for ΔC_{10}^μ, the identical chirality is not excluded at the 1σ region in S-I, and can be kept at the 2σ regions in all the 4 scenarios. A strict respect of the criterion line can be found for the WCs of two scalar operators (ΔC_S and ΔC_P) shown as (c) and (d) in Fig. 4. This indicates that the chirality is indistinguishable for the two muon type scalar operators, although their fitted sizes are SM-like. Due to the limited data about channels

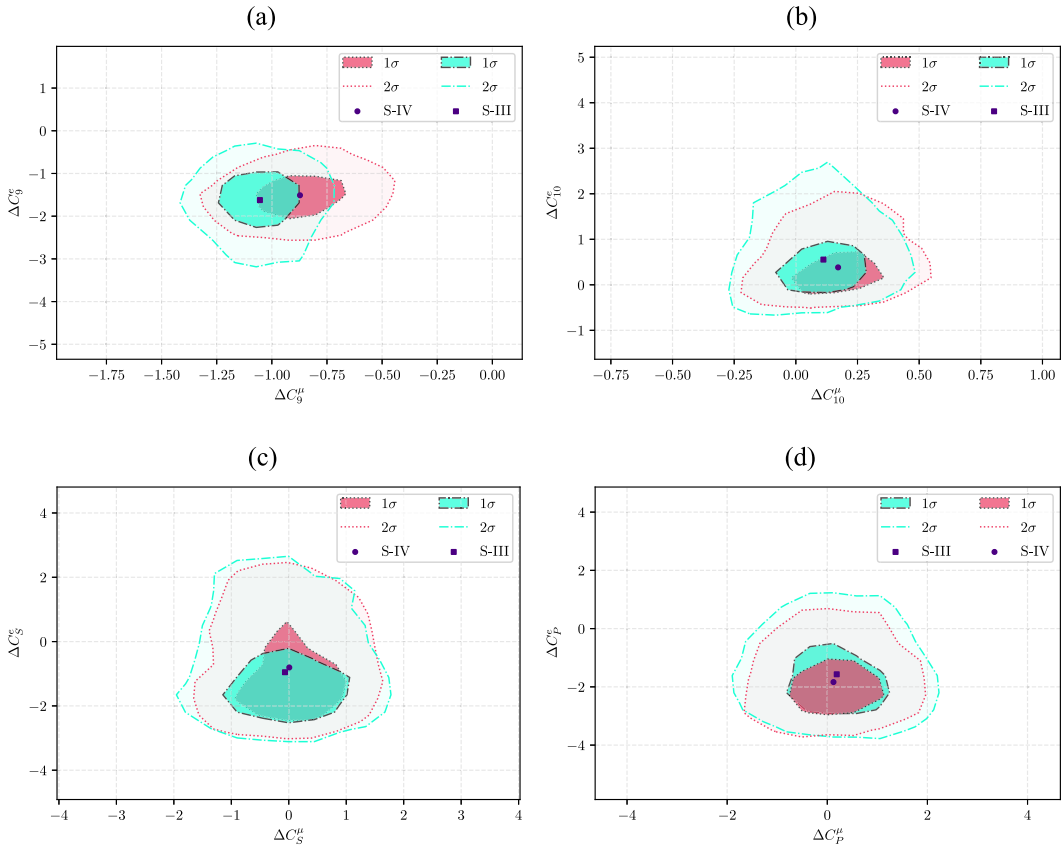

FIG. 3. The correlations of corresponding WCs ((a) to (d) stand for ΔC_9, ΔC_{10}, ΔC_S, and ΔC_P, respectively) specified by their lepton flavors with a consideration of $R_{K^{(*)}}^{2022}$, taking an example of left-handed operators. The red (dotted) and green (dot dashed) regions represent the S-IV as well as S-III, where darker/lighter part are their corresponding $1/2\sigma$ regions. Markers circle (square) are estimations of WCs in S-IV(S-III), respectively. The absence of S-II and S-I due to their WCs are not fully independent we set to be.

involving electrons, the surviving areas for $\Delta C_S^e - \Delta C_S'^e$ and $\Delta C_P^e - \Delta C_P'^e$ are much wider than the muon type operators, with the identical chirality line contained. Their sizes, which are consistent with SM at 2σ level, and the chirality relations are anticipated to be improved more precisely when more data is accumulated.

C. Discussions

Throughout the analyses in this work, the most important issue is whether the new physics possibility still exists by incorporating $R_{K^{(*)}}^{2022}$. As shown in Fig. 5 explicitly, although ΔC_{10} agrees with SM within 1σ in all the four scenarios for both muon and electron type, deviations from SM in ΔC_9^μ indeed exist for more than 4σ for most scenarios and ΔC_9^e for around 3σ in Scenario II.

The scalar operators are in general with small central values but large uncertainties as shown in Table III and IV. The 2-D correlations shown in Fig. 4 apparently indicate the strong linear relations

$$\Delta C_S^\mu = \Delta C_S'^\mu, \qquad \Delta C_P^\mu = \Delta C_P'^\mu. \tag{15}$$

On the other hand, if the emergence of new physics is described within the framework of SMEFT, the relations

$$\Delta C_S^\mu = -\Delta C_P^\mu, \qquad \Delta C_S'^\mu = \Delta C_P'^\mu \tag{16}$$

hold up to dimension-6 operators [70], leading to

$$\Delta C_S^{(\prime)\mu} = \Delta C_P^{(\prime)\mu} = 0. \tag{17}$$

Note this feature for null scalar operators may violate in other non-SMEFT new physics [71].

IV. CONCLUDING REMARKS

In this work, we perform global fits to two sets of datasets, one before and one after the release of $R_{K^{(*)}}^{2022}$ (denoted as dataset A and B), in four sets of working scenarios. In some of the working scenarios, we distinguish lepton flavor, which results in as many as 20 fitted parameters. Our numerical analysis based on Bayesian statistics helps to interpret data and the following points

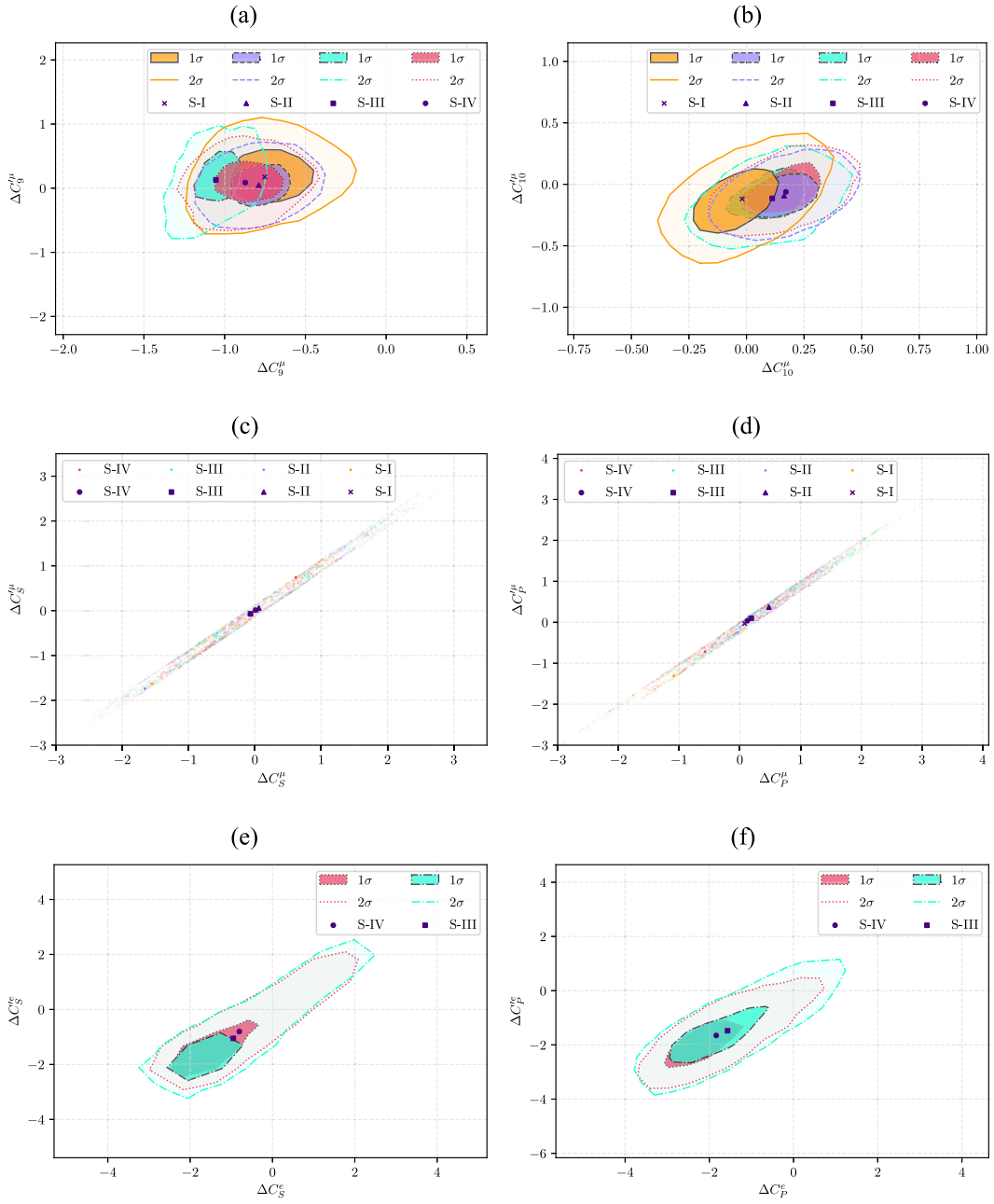

FIG. 4. The correlations of corresponding WCs distinct from their chirality incorporating the updated $R_{K^{(*)}}$, with a consideration of muon type operators [(a)–(d)] and typical electron type operators [(e)–(f)]. The orange (solid), purple (dashed), green (dot-dashed), and red (dotted) regions represent S-I, S-II, S-III, and S-IV, respectively. The description of absence of S-I and S-II follows the Fig. 3.

can be concluded incorporating $R_{K^{(*)}}^{2022}$. (i) The new physics possibility still exists. As explicitly shown in Fig. 5, current data still supports a deviation about or more than 4σ from SM for ΔC_9^{μ}. (ii) The interpretation of flavor dependence in WCs is improved. At 1σ level, the muon and electron flavor is distinguishable for $\Delta C_{9,S,P}$ but indistinguishable for ΔC_{10}. And if allowing 2σ errors, lepton flavor is indistinguishable for all the four operators and their corresponding WCs $\Delta C_{9,10,S,P}$. (iii) The relation between operators and their chiral dual ones is specified. The WCs for scalar operators ΔC_S^{μ} and ΔC_P^{μ} are strictly chirality independent. At 1σ level, the data also indicates that to distinguish chirality is not necessary for ΔC_S^{e} and ΔC_P^{e}. The WC ΔC_9^{μ} differs from its dual one $\Delta C_9^{\prime\mu}$ at 2σ level in all the four scenarios, while ΔC_{10}^{μ} distinguishes $\Delta C_{10}^{\prime\mu}$ in three of the four scenarios. (iv) If the emergence of new physics is in terms of SMEFT, the scalar operators vanish.

Although the working scenario dependence indeed exists by comparing with detailed scenarios, it does not change the main features of global fits. The obtained results from

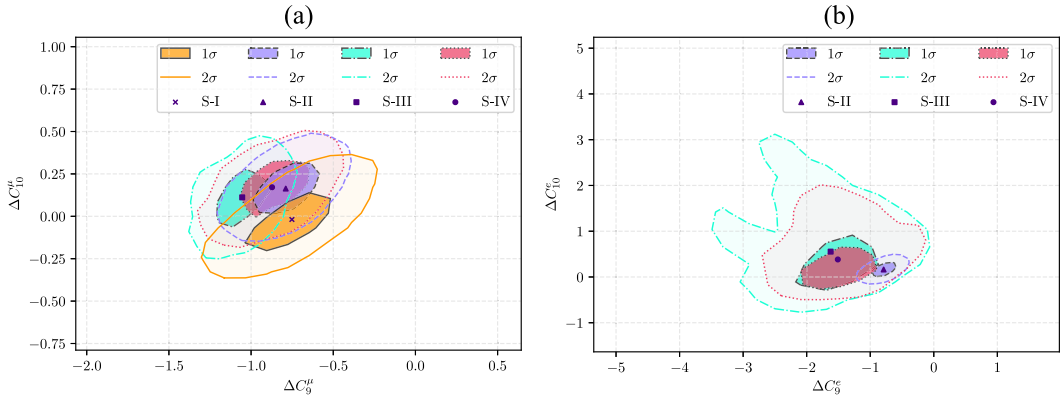

FIG. 5. The correlations of WCs involving more than 3σ deviations from SM predictions with the $R_{K^{(*)}}^{2022}$. Conventions of color, line types and markers remain the same as those in Figs. 3 and 4.

current model independent fits provide useful inputs for new physics models or help to discriminate some of the models.

ACKNOWLEDGMENTS

The authors benefited by discussions with Jibo He and Yue-Lin Sming Tsai. This work was supported by NSFC under Grant No. U1932104.

APPENDIX A: FORMULAS FOR INVOLVED OBSERVABLES

In this part, we provided a list about calculation of all observables we used in analysis, more detailed discussions are found in corresponding subsection.

1. $B_{s,d} \to \ell\ell$

It is worth pointing out that our formula deduced previously called CP-averaged or "experimental" branching ratio. The untagged or "theoretical" branching ratio is different from previous one through [72]

$$\mathrm{BR}^{\mathrm{untag}}(B_s \to \mu^+\mu^-) = \left[\frac{1+\mathcal{A}_{\Delta\Gamma} y_s}{1-y_s^2}\right]\mathrm{BR}(B_s \to \mu^+\mu^-),$$
$$\mathcal{A}_{\Delta\Gamma} = \frac{|k_P|^2\cos(2\varphi_P) - |k_S|^2\cos(2\varphi_S)}{|k_P|^2 + |k_S|^2}, \tag{A1}$$

with k_S, k_P, φ_S, φ_P which are given in [72].

2. $B \to V\ell^+\ell^-$ formulas

The full angular decay distribution of $\bar{B}^0 \to \bar{K}^{*0}\ell^+\ell^-$ which obtained from Buras [30] is shown as

$$\frac{\mathrm{d}^4\Gamma^{\ell}}{\mathrm{d}q^2\mathrm{d}\cos\theta_\ell\mathrm{d}\cos\theta_{K^*}\mathrm{d}\phi} = \frac{9}{32\pi}J^{\ell}(q^2,\theta_\ell,\theta_{K^*},\phi), \tag{A2}$$

where

$$\begin{aligned} J^{\ell}(q^2,\theta_\ell,\theta_{K^*},\phi) = {} & J_{1;s}^{\ell}\sin^2\theta_{K^*} + J_{1;c}^{\ell}\cos_{K^*}^{\theta} + (J_{2;s}^{\ell}\sin^2\theta_{K^*} + J_{2;c}^{\ell}\cos^2\theta_{K^*})\cos 2\theta_\ell + J_3^{\ell}\sin^2\theta_{K^*}\sin^2\theta_\ell\cos 2\phi \\ & + J_4^{\ell}\sin 2\theta_{K^*}\sin 2\theta_\ell\cos\phi + J_5^{\ell}\sin 2\theta_{K^*}\sin\theta_\ell\cos\phi + (J_{6;s}^{\ell}\sin^2\theta_{K^*} + J_{6;c}^{\ell}\cos^2\theta_{K^*})\cos\theta_\ell \\ & + J_7^{\ell}\sin 2\theta_{K^*}\sin\theta_\ell\sin\phi + J_8^{\ell}\sin 2\theta_{K^*}\sin 2\theta_\ell\sin\phi + J_9^{\ell}\sin^2\theta_{K^*}\sin^2\theta_\ell\sin 2\phi \end{aligned} \tag{A3}$$

The corresponding expression for the CP-conjugated mode $B^0 \to K^{*0}\ell^+\ell^-$ is obtained form Eq. (A3) by the replacements $J_{1,2,3,4,7;(a)}^{\ell} \to \bar{J}_{1,2,3,4,7;(a)}^{\ell}$, $J_{5,6,8,9;(a)}^{\ell} \to -\bar{J}_{5,6,8,9;(a)}^{\ell}$. With the eight transverse amplitudes defined in the consecutive subsection, the angular coefficients J_i in (7) can be written as

$$
\begin{aligned}
J^{\ell}_{1;s} &= \frac{(2+\beta^2_\ell)}{4}[|A^{\mathrm{L}}_{\perp;\ell}|^2 + |A^{\mathrm{L}}_{\parallel;\ell}|^2 + (\mathrm{L}\to\mathrm{R})] + \frac{4m^2_\ell}{q^2}\Re(A^{\mathrm{L}}_{\perp;\ell}A^{\mathrm{R}^*}_{\perp;\ell} + A^{\mathrm{L}}_{\parallel;\ell}A^{\mathrm{R}^*}_{\parallel;\ell}),\\
J^{\ell}_{1;c} &= |A^{\mathrm{L}}_{0;\ell}|^2 + |A^{\mathrm{R}}_{0;\ell}|^2 + \frac{4m^2_\ell}{q^2}[|A_{t;\ell}|^2 + 2\Re(A^{\mathrm{L}}_{0;\ell}A^{\mathrm{R}*}_{0;\ell})] + \beta^2_\ell|A_{\mathrm{S};\ell}|^2,\\
J^{\ell}_{2;s} &= \frac{\beta^2_\ell}{4}[|A^{\mathrm{L}}_{\perp;\ell}|^2 + |A^{\mathrm{L}}_{\parallel;\ell}|^2 + (\mathrm{L}\to\mathrm{R})], \qquad J^{\ell}_{2;c} = -\beta^2_\ell[|A^{\mathrm{L}}_{0;\ell}|^2 + (\mathrm{L}\to\mathrm{R})],\\
J^{\ell}_{3} &= \frac{1}{2}\beta^2_\ell[|A^{\mathrm{L}}_{\perp;\ell}|^2 - |A^{\mathrm{L}}_{\parallel;\ell}|^2 + (\mathrm{L}\to\mathrm{R})], \qquad J^{\ell}_{4} = \frac{1}{\sqrt{2}}\beta^2_\ell[\Re(A^{\mathrm{L}}_{0;\ell}A^{\mathrm{L}*}_{\parallel;\ell}) + (\mathrm{L}\to\mathrm{R})],\\
J^{\ell}_{5} &= \sqrt{2}\beta_\ell\left[\Re(A^{\mathrm{L}}_{0;\ell}A^{\mathrm{L}*}_{\perp;\ell}) - (\mathrm{L}\to\mathrm{R}) - \frac{m_\ell}{\sqrt{q^2}}\Re(A^{\mathrm{L}}_{\parallel;\ell}A^{*}_{\mathrm{S};\ell} + A^{\mathrm{R}}_{\parallel;\ell}A^{*}_{\mathrm{S};\ell})\right],\\
J^{\ell}_{6;s} &= 2\beta_\ell[\Re(A^{\mathrm{L}}_{\parallel;\ell}A^{\mathrm{L}^*}_{\perp;\ell}) - (\mathrm{L}\to\mathrm{R})], \qquad J^{\ell}_{6;c} = 4\beta_\ell\frac{m_\ell}{\sqrt{q^2}}[\Re(A^{\mathrm{L}}_{0;\ell}A^{*}_{\mathrm{S};\ell}) + (\mathrm{L}\to\mathrm{R})],\\
J^{\ell}_{7} &= \sqrt{2}\beta_\ell\left[\Im(A^{\mathrm{L}}_{0;\ell}A^{\mathrm{L}*}_{\parallel;\ell}) - (\mathrm{L}\to\mathrm{R}) + \frac{m_\ell}{\sqrt{q^2}}\Im(A^{\mathrm{L}}_{\perp;\ell}A^{*}_{\mathrm{S};\ell} + A^{\mathrm{R}}_{\perp;\ell}A^{*}_{\mathrm{S};\ell})\right],\\
J^{\ell}_{8} &= \frac{1}{\sqrt{2}}\beta^2_\ell[\Im(A^{\mathrm{L}}_{0;\ell}A^{\mathrm{L}*}_{\perp;\ell}) + (\mathrm{L}\to\mathrm{R})], \qquad J^{\ell}_{9} = \beta^2_\ell[\Im(A^{\mathrm{L}*}_{\parallel;\ell}A^{\mathrm{L}}_{\perp;\ell}) + (\mathrm{L}\to\mathrm{R})],\\
S_{i;a} &= (J_{i;a} + \bar{J}_{i;a})/\frac{d(\Gamma+\bar{\Gamma})}{dq^2},
\end{aligned}
\tag{A4}
$$

which further rely on various helicity amplitudes, giving

$$
\begin{aligned}
A^{\mathrm{L,R}}_{\perp;\ell} &= N^{\ell}_0\sqrt{2}\lambda M^2_B\left[[(C^{\ell}_9 + C'^{\ell}_9) \mp (C^{\ell}_{10} + C'^{\ell}_{10})]\frac{V(q^2)}{M_B + M_{K^*}} + \frac{2m_b}{q^2}(C^{\ell}_7 + C'^{\ell}_7)T_1(q^2)\right] + \Delta A^{\mathrm{L,R}}_{\perp},\\
A^{\mathrm{L,R}}_{\parallel;\ell} &= -N^{\ell}_0\sqrt{2}(M^2_B - M^2_{K^*})\left[[(C^{\ell}_9 - C'^{\ell}_9) \mp (C^{\ell}_{10} - C'^{\ell}_{10})]\frac{A_1(q^2)}{M_B - M_{K^*}} + \frac{2m_b}{q^2}(C^{\ell}_7 - C'^{\ell}_7)T_2(q^2)\right] + \Delta A^{\mathrm{L,R}}_{\parallel},\\
A^{\mathrm{L,R}}_{0;\ell} &= \frac{-N^{\ell}_0}{2M_{K^*}\sqrt{q^2}}\left\{[(C^{\ell\prime}_9 - C'^{\ell}_9) \mp (C^{\ell}_{10} - C'^{\ell}_{10})]\left[(M^2_B - M^2_{K^*} - q^2)(M_B + M_{K^*})A_1(q^2) - \lambda^2 M^4_B\frac{A_2(q^2)}{M_B + M_{K^*}}\right]\right.\\
&\quad \left. + 2m_b(C^{\ell}_7 - C'^{\ell}_7)\left[(M^2_B + 3M^2_{K^*} - q^2)T_2(q^2) - \frac{\lambda^2 M^4_B}{M^2_B - M^2_{K^*}}T_3(q^2)\right]\right\} + \Delta A^{\mathrm{L,R}}_{0},\\
A_{t;\ell} &= \frac{N^{\ell}_0}{\sqrt{q^2}}\lambda M^2_B\left[2(C^{\ell}_{10} - C'^{\ell}_{10}) + \frac{q^2}{m_\ell}(C^{\ell}_P - C'^{\ell}_P)\right]A_0(q^2),\\
A_{\mathrm{S};\ell} &= -2N^{\ell}_0\lambda M^2_B(C^{\ell}_{\mathrm{S}} - C'^{\ell}_{\mathrm{S}})A_0(q^2),
\end{aligned}
\tag{A5}
$$

associated with the constant

$$
N^0_\ell = V_{tb}V^*_{ts}\left[\frac{G^2_F\alpha^2}{3\times 2^{10}\pi^5 M_B}q^2\lambda\beta_\ell\right]^{\frac{1}{2}}
\tag{A6}
$$

and parameters λ and β_μ defined as

$$
\beta_\ell = \sqrt{1 - 4\frac{m^2_\ell}{q^2}}, \qquad \lambda(q^2, M^2_K) = \left[\left(1 - \frac{q^2}{M^2_B}\right)^2 - 2\frac{m^2_K}{M^2_B}\left(1 + \frac{q^2}{M^2_B}\right) + \frac{m^4_K}{M^4_B}\right]^{\frac{1}{2}}.
$$

The corrections ΔA in Eq. (A5), originating from weak annihilation and spectator scattering [41], are given as

$$\Delta A_{\perp}^{L;R} = \frac{2\sqrt{2}\lambda N m_b M_B^2}{q^2}\left(\mathcal{T}_{\perp}^{(t),\mathrm{nf+WA}} + \frac{\lambda_u}{\lambda_t}\mathcal{T}_{\perp}^{(u)}\right),$$
$$\Delta A_{\parallel}^{L;R} = \frac{-2\sqrt{2}E_V N m_b (M_B^2 - M_V^2)}{q^2 M_B}\left(\mathcal{T}_{\perp}^{(t),\mathrm{nf+WA}} + \frac{\lambda_u}{\lambda_t}\mathcal{T}_{\perp}^{(u)}\right),$$
$$\Delta A_0^{L;R} = -\frac{N M_B^2 m_b}{\sqrt{q^2} M_V}\left\{\left[(M_B^2 + 3M_V^2 - q^2)\frac{2E_V}{M_B^3} - \frac{\lambda^2 M_B^2}{M_B^2 - M_V^2}\right] \times \left(\mathcal{T}_{\perp}^{(t),\mathrm{nf+WA}} + \frac{\lambda_u}{\lambda_t}\mathcal{T}_{\perp}^{(u)}\right) - \frac{\lambda^2 M_B^2}{M_B^2 - M_V^2} \times \left(\mathcal{T}_{\parallel}^{(t),\mathrm{nf+WA}} + \frac{\lambda_u}{\lambda_t}\mathcal{T}_{\parallel}^{(u)}\right)\right\}, \tag{A7}$$

with $\lambda_i \equiv V_{ib}V_{is}^*$ and $E_V = \frac{M_B^2 + M_V^2 - q^2}{2M_B}$. The amplitudes $\mathcal{T}_{\perp,\parallel}$ in Eq. (A7), containing contributions from both nonfactorizable hard-spectator scattering and weak annihilation, can be obtained by subtracting factorizable contributions from the invariant amplitude calculated in QCDF [21,22,73], giving

$$\mathcal{T}_a = \xi_a C_a + \frac{\pi^2}{N_c}\frac{f_B f_{V,a}}{MB}\Xi_a \sum_{\pm}\int_0^{\infty}\frac{d\omega}{\omega}\Phi_{B,\pm}(\omega)\int_0^1 du \Phi_{K^*,a}(u) T_{a,\pm}(u,\omega) \tag{A8}$$

with $\Xi_{\parallel} = \frac{M_V}{E_V}$, $\Xi_{\perp} = 1$, $N_c = 3$ and

$$C_a = C_a^{(0)} + \frac{\alpha_s C_F}{4\pi} C_a^{(1)},$$
$$T_{a,\pm} = T_{a,\pm}^{(0)} + \frac{\alpha_s C_F}{4\pi} T_{a,\pm}^{(1)}. \tag{A9}$$

In this work, we do not incorporate the long-distance effect generated from charm-loop, which has been considered in [74,75]. In large energy limit (LEL), the number of heavy-to-light transition form factors can be reduced from 7 to 2, corresponding to transversal and longitudinal polarization of K^*. The correspondence between the two sets of form factors [76] is given as

$$V(q^2) = \left(1 + \frac{M_{\mathrm{vec}}}{M}\right)\xi_{\perp}, \qquad A_1(q^2) = \frac{2E}{M + M_{\mathrm{vec}}}\xi_{\perp},$$
$$A_2(q^2) = \left(1 + \frac{M_{\mathrm{vec}}}{M}\right)\left[\xi_{\perp} - \frac{M_{\mathrm{vec}}}{E}\xi_{\parallel}\right], \qquad A_0(q^2) = \left(1 - \frac{M_{\mathrm{vec}}^2}{ME}\right)\xi_{\parallel} + \frac{M_{\mathrm{vec}}}{M}\xi_{\perp},$$
$$T_1(q^2) = \xi_{\perp}, \qquad T_2(q^2) = \left(1 - \frac{q^2}{M^2 - M_{\mathrm{vec}}^2}\right)\xi_{\perp}, \qquad T_3(q^2) = \xi_{\perp} - \frac{M_{\mathrm{vec}}}{E}\left(1 - \frac{M_{\mathrm{vec}}^2}{M^2}\right)\xi_{\parallel}, \tag{A10}$$

where M and M_{vec} stand for B mesons as well as final state vector mesons, respectively. To solve $\xi_{\perp}$ and $\xi_{\parallel}$, we use form factors T_1 and A_0 [69] in the form of simplified series expansion (SSE) in our practical analysis.

3. $B \to P\ell^+\ell^-$

The angular distribution functions are described below [77]:

$$I_a^{\ell}(q^2; C'_{7,8,9,10,S,P}) = \frac{q^2}{M_B^4}(\beta_{\ell}^3|F_S^{\ell}|^2 + \beta_{\ell}|F_P^{\ell}|^2) + \frac{\lambda}{4}\left(\lambda\beta_{\ell}|C_{10}^{\ell}|^2 + \lambda\beta_{\ell}\left|C_9^{\ell} + \frac{2m_b\mathcal{T}_P^{(0)}}{M_B\xi_P}\right|^2\right) + \frac{2m_{\ell}\beta_{\ell}(M_B^2 - M_K^2 + q^2)\Re(F_P^{\ell}F_A^{\ell *})}{M_B^4} + \frac{4m_{\ell}^2\beta_{\ell}|F_A^{\ell}|^2}{M_B^2},$$
$$I_c^{\ell}(q^2; C'_{7,8,9,10}) = -\frac{\lambda}{4}\left(\lambda\beta_{\ell}^3|C_{10}^{\ell}|^2 + \lambda\beta_{\ell}^3\left|C_9^{\ell} + \frac{2m_b\mathcal{T}_P}{M_B\xi_P}\right|^2\right), \tag{A11}$$

where form factors are defined as

$$
\begin{aligned}
&F_A^\ell = C_{10}^\ell, \qquad F_T^\ell = 0, \qquad F_{T5}^\ell = 0,\\
&F_P^\ell = \frac{M_B^2 - M_K^2}{2m_b(m_b - m_s)} \frac{f_0}{f_+}(C_P^\ell + C_P'^\ell) + m_l C_{10}^\ell \left[\frac{M_B^2 - M_K^2}{q^2}\left(\frac{2E}{M_B} - 1\right) - 1\right],\\
&F_S^\ell = \frac{M_B^2 - M_K^2}{2m_b(m_b - m_s)} \frac{f_0(q^2)}{f_+(q^2)}(C_S^\ell + C_S'^\ell),\\
&F_V^\ell = C_9^\ell + \frac{2m_b}{M_B}\frac{\mathcal{T}_P(q^2)}{\xi_P(q^2)}, \qquad \frac{f_0}{f_+} = \frac{2E}{M_B}\left[1 + \mathcal{O}(\alpha_s) + \mathcal{O}\left(\frac{q^2}{M_B^2}\sqrt{\frac{\Lambda_{\rm QCD}}{E}}\right)\right].
\end{aligned}
\tag{A12}
$$

The invariant amplitude $\mathcal{T}_P$ has the form similar with $\mathcal{T}_\parallel$ in $B \to V\ell^+\ell^-$ [22]. We preserve the leading order and next-leading order nonfactorizable contribution, giving

$$
\begin{aligned}
\mathcal{T}_P(q^2) = \xi_P &\left[(C_7^{\rm eff} + C_7'^{\rm eff}) + \frac{M_B}{2m_b} Y(q^2) + \frac{\alpha_s C_F}{4\pi} C_\parallel^{nf}\right]\\
&+ \frac{\pi^2}{N_c}\frac{f_B f_P}{M_B}\sum_\pm \int_0^\infty \frac{d\omega}{\omega}\Phi_{B,\pm}(\omega)\int_0^1 du \Phi_{K,\parallel}(u)\left[T_{\parallel,\pm}^{(0)} + \frac{\alpha_s C_F}{4\pi}(T_{\parallel,\pm}^{(nf)})\right](u,\omega).
\end{aligned}
\tag{A13}
$$

The form factors based on SSE [68,74] can be parametrized as

$$
\begin{aligned}
&\xi_P = f_+(q^2) \equiv \frac{f_+(0)}{1 - q^2/m_{\rm res+}^2}\left\{1 + a_+^1\left[z(q^2) - z(0) + \frac{1}{2}(z(q^2)^2 - z(0)^2)\right]\right\},\\
&z(q^2) = \frac{\sqrt{\tau_+ - q^2} - \sqrt{\tau_+ - \tau_0}}{\sqrt{\tau_+ - q^2} + \sqrt{\tau_+ - \tau_0}}, \qquad \tau_0 = \sqrt{\tau_+}(\sqrt{\tau_+} - \sqrt{\tau_+ - \tau_-}), \qquad \tau_\pm = (M_B \pm M_P)^2,
\end{aligned}
\tag{A14}
$$

in which $f_+(q^2 = 0)$ can be calculated by LCSR and listed in Table II.

4. $B \to X_s\ell^+\ell^-$

Here we give the definition of the important function $\tilde{N}$ in Eq. (8),

$$
\begin{aligned}
\tilde{N} \equiv &\left(1 + \frac{2\hat{m}_\ell^2}{\hat{s}}\right)\left[|C_9^{\rm new}|^2(1 + 2\hat{s})\left(1 + \frac{\alpha_s}{\pi}\tau_{99}(\hat{s})\right) + 4|C_7^{\rm new}|^2\left(1 + \frac{2}{\hat{s}}\right)\left(1 + \frac{\alpha_s}{\pi}\tau_{77}(\hat{s})\right)\right.\\
&\left. + 12\Re(C_7^{\rm new} C_9^{\rm new*})\left(1 + \frac{\alpha_s}{\pi}\tau_{79}(\hat{s})\right)\right] + |C_{10}^{\rm new}|^2\left[(1 + 2\hat{s}) + \frac{2\hat{m}_\ell^2}{\hat{s}}(1 - 4\hat{s})\right]\left(1 + \frac{\alpha_s}{\pi}\tau_{99}(\hat{s})\right)\\
&+ \frac{3}{2}|m_b C_S|^2(\hat{s} - 4\hat{m}_\ell^2) + \frac{3}{2}|m_b C_P|^2\hat{s} + 6\Re(m_b C_{10}^{\rm new} C_P^*)\hat{m}_\ell + (C_i \leftrightarrow C_i'),
\end{aligned}
\tag{A15}
$$

where $\hat{m}_\ell$, $\hat{s}$, and z has the form of

$$
\hat{m}_\ell \equiv \frac{m_\ell}{m_{b;\rm pole}}, \qquad \hat{s} \equiv \frac{s}{m_{b;\rm pole}^2}, \qquad z \equiv \frac{m_{c;\rm pole}^2}{m_{b;\rm pole}^2}
\tag{A16}
$$

and τ_{77}, τ_{79}, and τ_{99} have been calculated in [43]. Especially, $C_7^{\rm new}$ and $C_9^{\rm new}$ are defined as

$$C_7^{\rm new}(s) = \left(1+\frac{\alpha_s}{\pi}\sigma_7(s)\right)C_7^{\rm eff} - \frac{\alpha_s}{4\pi}\left[C_1F_1^{(7)}(s)+C_2F_2^{(7)}(s)+C_8^{\rm eff}F_8^{(7)}(s)\right],$$
$$C_9^{\rm new}(s) = \left(1+\frac{\alpha_s}{\pi}\sigma_9(s)\right)C_9^{\rm eff} - \frac{\alpha_s}{4\pi}\left[C_1F_1^{(9)}(s)+C_2F_2^{(9)}(s)+C_8^{\rm eff}F_8^{(9)}(s)\right],$$
$$C_9^{\rm new}(s) = \left(1+\frac{\alpha_s}{\pi}\sigma_9(s)\right)C_{10}^{\rm eff}, \tag{A17}$$

with σ_7, σ_9 given in [43] as well, and $F_{1;2;8}^{(7;9)}$ introduced in [22]. All the analytical formulas are well summarized in [41].

5. $\Lambda_b \to \Lambda\ell^+\ell^-$

With naive factorization approximation, the 10 angular distribution function in bottomed baryon decays can be expressed as,

$$J_{1ss} = \frac{1}{4}[|A_{\perp_1}^R|^2+|A_{\parallel_1}^R|^2+2|A_{\perp_0}^R|^2+2|A_{\parallel_0}^R|^2+(R\leftrightarrow L)],$$
$$J_{2ss} = \frac{\alpha_\Lambda}{2}\Re\{A_{\perp_1}^R A_{\parallel_1}^{*R}+2A_{\perp_0}^R A_{\parallel 0}^{*R}+(R\leftrightarrow L)\},$$
$$J_{1cc} = \frac{1}{2}[|A_{\perp_1}^R|^2+|A_{\parallel_1}^R|^2+(R\leftrightarrow L)], \qquad J_{1c} = -\Re\{A_{\perp_1}^R A_{\parallel_1}^{*R}-(R\leftrightarrow L)\},$$
$$J_{2cc} = +\alpha_\Lambda\Re\{A_{\perp_1}^R A_{\parallel_1}^{*R}+(R\leftrightarrow L)\}, \qquad J_{2c} = -\frac{\alpha_\Lambda}{2}[|A_{\perp_1}^R|^2+|A_{\parallel_1}^R|^2-(R\leftrightarrow L)],$$
$$J_{3sc} = +\frac{\alpha_\Lambda}{\sqrt{2}}\Im\{A_{\perp_1}^R A_{\perp_0}^{*R}-A_{\parallel_1}^R A_{\parallel_0}^{*R}+(R\leftrightarrow L)\}, \qquad J_{3s} = \frac{\alpha_\Lambda}{\sqrt{2}}\Re\{A_{\perp_1}^R A_{\parallel_0}^{*R}-A_{\parallel_1}^R A_{\perp_0}^{*R}+(R\leftrightarrow L)\},$$
$$J_{4sc} = +\frac{\alpha_\Lambda}{\sqrt{2}}\Im\{A_{\perp_1}^R A_{\perp_0}^{*R}-A_{\parallel_1}^R A_{\parallel_0}^{*R}-(R\leftrightarrow L)\}, \qquad J_{4s} = \frac{\alpha_\Lambda}{\sqrt{2}}\Re\{A_{\perp_1}^R A_{\parallel_0}^{*R}-A_{\parallel_1}^R A_{\perp_0}^{*R}-(R\leftrightarrow L)\},$$

where α_Λ given in [58] and presented in Table I. The definition of amplitudes A can be further defined based on helicity amplitudes, giving

$$A_{\perp_0}^{L(R)} = +\sqrt{2}N_1\left(C_{9,10,+}^{L(R)}H_0^V(+1/2,+1/2)-\frac{2m_b(C_7+C_7')}{q^2}H_0^T(+1/2,+1/2)\right),$$
$$A_{\parallel_0}^{L(R)} = -\sqrt{2}N_1\left(C_{9,10,-}^{L(R)}H_0^A(+1/2,+1/2)+\frac{2m_b(C_7-C_7')}{q^2}H_0^{T5}(+1/2,+1/2)\right),$$
$$A_{\perp_1}^{L(R)} = +\sqrt{2}N_1\left(C_{9,10,+}^{L(R)}H_+^V(-1/2,+1/2)-\frac{2m_b(C_7+C_7')}{q^2}H_+^T(-1/2,+1/2)\right),$$
$$A_{\parallel_1}^{L(R)} = -\sqrt{2}N_1\left(C_{9,10,-}^{L(R)}H_+^A(-1/2,+1/2)+\frac{2m_b(C_7-C_7')}{q^2}H_+^{T5}(-1/2,+1/2)\right), \tag{A18}$$

with modified WCs and constant N_1

$$C_{9,10,+}^{L(R)} = (C_9\mp C_{10})+(C_9'\mp C_{10}'), \qquad C_{9,10,-}^{L(R)}(C_9\mp C_{10})-(C_9'\mp C_{10}'),$$
$$N_1 = G_F V_{tb}V_{ts}^*\alpha_e\sqrt{\frac{q^2\lambda}{3\times 2^{11}m_{\Lambda_b}\pi^5}},$$

and helicity amplitudes

$$
\begin{aligned}
H_t^V(+1/2,+1/2) &= H_t^V(-1/2,-1/2) = f_t^V(q^2)\frac{m_{\Lambda_b}-m_\Lambda}{\sqrt{q^2}}\sqrt{s_+},\\
H_0^V(+1/2,+1/2) &= H_0^V(-1/2,-1/2) = f_0^V(q^2)\frac{m_{\Lambda_b}+m_\Lambda}{\sqrt{q^2}}\sqrt{s_-},\\
H_+^V(-1/2,+1/2) &= H_-^V(+1/2,-1/2) = -f_\perp^V(q^2)\sqrt{2s_-},\\
H_t^A(+1/2,+1/2) &= -H_t^A(-1/2,-1/2) = f_t^A(q^2)\frac{m_{\Lambda_b}+m_\Lambda}{\sqrt{q^2}}\sqrt{s_-},\\
H_0^A(+1/2,+1/2) &= -H_0^A(-1/2,-1/2) = f_0^A(q^2)\frac{m_{\Lambda_b}-m_\Lambda}{\sqrt{q^2}}\sqrt{s_+},\\
H_+^A(-1/2,+1/2) &= -H_-^A(+1/2,-1/2) = -f_\perp^A(q^2)\sqrt{2s_+},\\
H_0^T(+1/2,+1/2) &= -H_0^T(-1/2,-1/2) = -f_0^T\sqrt{q^2}\sqrt{s_-},\\
H_+^T(-1/2,+1/2) &= -H_-^T(+1/2,-1/2) = f_\perp^T(q^2)(m_{\Lambda_b}+m_\Lambda)\sqrt{2s_-},\\
H_0^{T5}(+1/2,+1/2) &= -H_0^{T5}(-1/2,-1/2) = f_0^{T5}\sqrt{q^2}\sqrt{s_+},\\
H_+^{T5}(-1/2,+1/2) &= -H_-^{T5}(+1/2,-1/2) = -f_\perp^{T5}(q^2)(m_{\Lambda_b}-m_\Lambda)\sqrt{2s_+}.
\end{aligned}
\tag{A19}
$$

The form factors can be parametrized as

$$
f_i(q^2) = \frac{1}{1-q^2/(m_{\text{pole}}^{f_i})^2}[a_0^{f_i}+a_1^{f_i}z(q^2)]. \tag{A20}
$$

and the detailed input parameters $a_{0,1}$ have been listed in Table II.

APPENDIX B: EXPERIMENTAL DATA FOR RELATED OBSERVABLES

Here we summarize all the experimental results related to our analysis. The number of observables is 203 at total for new data, dataset B, and 201 for dataset A. The former one can be obtained via replacing old $R_{K^{(*)}}$ and the branching fraction of the corresponding electron mode in the latter by the latest LHCb results [20]. The detailed values have been presented in the following three tables (Tables V–VII) while the SM predictions in the second to the last column are calculated by our code supporting this analysis.

TABLE V. The differential branching fractions part of dataset A in the unit of GeV^{-2}.

Observable	q^2 (GeV^2)	Experimental value	This work	*Flavio* [49]
		LHCb ($B^+ \to K^+\ell^+\ell^-$) [10]		
R_K	[1.1, 6.0]	$0.846^{+0.042+0.013}_{-0.039-0.012}$	1.000 ± 0.000	1.001 ± 0.000
$10^8 d\mathcal{B}/dq^2\vert_{(K^+e^+e^-)}$	[1.1, 6.0]	$2.86^{+0.15+0.13}_{-0.14-0.13}$	3.647 ± 1.147	3.484 ± 0.647
		LHCb ($B \to K^{(*)}\ell^+\ell^-$) [11]		
$R_{K^{*+}}$	[0.045, 6.0]	$0.70^{+0.18+0.03}_{-0.13-0.04}$	0.974 ± 0.000	0.972 ± 0.003
R_{K_S}	[1.1, 6.0]	$0.66^{+0.20+0.02}_{-0.14-0.04}$	1.000 ± 0.000	1.001 ± 0.000
$10^8 d\mathcal{B}/dq^2\vert_{(K^0e^+e^-)}$	[1.1, 6.0]	$2.6^{+0.6+0.1}_{-0.6-0.1}$	3.383 ± 1.045	3.230 ± 0.531
$10^8 d\mathcal{B}/dq^2\vert_{(K^{*+}e^+e^-)}$	[0.045, 6.0]	$9.2^{+1.9+0.8}_{-1.8-0.6}$	5.639 ± 1.036	6.539 ± 0.966
		LHCb ($B^0 \to K^{*0}\ell^+\ell^-$) [12]		
$R_{K^{*0}}$	[0.045, 1.1]	$0.66^{+0.11}_{-0.07} \pm 0.03$	0.931 ± 0.000	0.925 ± 0.005
	[1.1, 6.0]	$0.69^{+0.11}_{-0.07} \pm 0.05$	0.996 ± 0.000	0.996 ± 0.001

(Table continued)

TABLE V. *(Continued)*

Observable	q^2 (GeV^2)	Experimental value	This work	*Flavio* [49]
		Belle $(B \to K^* \ell^+ \ell^-)$ [5]		
$R_{K^{*+}}$	[0.045, 1.1]	$0.62^{+0.60}_{-0.36} \pm 0.09$	0.932 ± 0.000	0.925 ± 0.005
	[1.1, 6.0]	$0.72^{+0.99}_{-0.44} \pm 0.15$	0.996 ± 0.000	0.996 ± 0.001
$10^7\mathcal{B}(K^{*+}e^+e^-)$	[1.1, 6.0]	$1.7^{+1.0}_{-1.0} \pm 0.2$	2.227 ± 0.464	2.546 ± 0.396
$10^7\mathcal{B}(K^{*+}\mu^+\mu^-)$	[1.1, 6.0]	$1.2^{+0.9}_{-0.7} \pm 0.2$	2.219 ± 0.465	2.537 ± 0.344
$R_{K^{*0}}$	[0.045, 1.1]	$0.46^{+0.55}_{-0.27} \pm 0.13$	0.931 ± 0.000	0.925 ± 0.004
	[1.1, 6.0]	$1.06^{+0.63}_{-0.38} \pm 0.13$	0.996 ± 0.000	0.996 ± 0.001
$10^7\mathcal{B}(K^{*0}e^+e^-)$	[1.1, 6.0]	$1.8^{+0.6}_{-0.6} \pm 0.2$	2.035 ± 0.430	2.331 ± 0.338
$10^7\mathcal{B}(K^{*0}\mu^+\mu^-)$	[1.1, 6.0]	$1.9^{+0.6}_{-0.5} \pm 0.3$	2.028 ± 0.426	2.323 ± 0.317
		Belle $(B \to K^* \gamma)$ [55]		
$10^5\mathcal{B}(K^{*0}\gamma)$		$4.5 \pm 0.3 \pm 0.2$	4.146 ± 0.420	4.202 ± 0.761
$10^5\mathcal{B}(K^{*+}\gamma)$		$5.2 \pm 0.4 \pm 0.3$	4.474 ± 0.454	4.271 ± 0.792
		Belle $(B^+ \to K^+ \ell^+ \ell^-)$ [6]		
$10^7\mathcal{B}(K^+\mu^+\mu^-)$	[0.1, 4.0]	$1.76^{+0.41}_{-0.37} \pm 0.04$	1.444 ± 0.434	1.370 ± 0.222
$10^7\mathcal{B}(K^0_S\mu^+\mu^-)$	[0.1, 4.0]	$0.62^{+0.30}_{-0.23} \pm 0.02$	0.670 ± 0.202	0.635 ± 0.111
$10^7\mathcal{B}(K^+e^+e^-)$	[0.1, 4.0]	$1.80^{+0.33}_{-0.30} \pm 0.05$	1.446 ± 0.442	1.371 ± 0.232
$10^7\mathcal{B}(K^0_Se^+e^-)$	[0.1, 4.0]	$0.38^{+0.25}_{-0.19} \pm 0.01$	0.671 ± 0.201	0.636 ± 0.115
R_{K^+}	[0.1, 4.0]	$0.98^{+0.29}_{-0.26} \pm 0.02$	0.999 ± 0.000	0.999 ± 0.000
$R_{K^0_S}$	[0.1, 4.0]	$1.62^{+1.31}_{-1.01} \pm 0.02$	0.999 ± 0.000	0.999 ± 0.000
$10^7\mathcal{B}(K^+\mu^+\mu^-)$	[1.0, 6.0]	$2.30^{+0.41}_{-0.38} \pm 0.05$	1.825 ± 0.570	1.744 ± 0.268
$10^7\mathcal{B}(K^0_S\mu^+\mu^-)$	[1.0, 6.0]	$0.31^{+0.22}_{-0.16} \pm 0.01$	0.846 ± 0.264	0.808 ± 0.138
$10^7\mathcal{B}(K^+e^+e^-)$	[1.0, 6.0]	$1.66^{+0.32}_{-0.29} \pm 0.04$	1.825 ± 0.581	1.743 ± 0.308
$10^7\mathcal{B}(K^0_Se^+e^-)$	[1.0, 6.0]	$0.56^{+0.25}_{-0.20} \pm 0.02$	0.846 ± 0.265	0.808 ± 0.132
R_{K^+}	[1.0, 6.0]	$1.39^{+0.36}_{-0.33} \pm 0.02$	1.000 ± 0.000	1.001 ± 0.000
$R_{K^0_S}$	[1.0, 6.0]	$0.55^{+0.46}_{-0.34} \pm 0.01$	1.000 ± 0.000	1.001 ± 0.000
		LHCb $(B^+ \to K^+\mu^+\mu^-)$ [13]		
$10^9 d\mathcal{B}/dq^2$	[1.1, 2.0]	$23.3 \pm 1.5 \pm 1.2$	37.243 ± 11.219	35.256 ± 6.385
	[2.0, 3.0]	$28.2 \pm 1.6 \pm 1.4$	36.911 ± 11.308	35.095 ± 6.056
	[3.0, 4.0]	$25.4 \pm 1.5 \pm 1.3$	36.540 ± 11.480	34.908 ± 6.329
	[4.0, 5.0]	$22.1 \pm 1.4 \pm 1.1$	36.128 ± 11.715	34.689 ± 5.610
	[5.0, 6.0]	$23.1 \pm 1.4 \pm 1.2$	35.664 ± 11.996	34.429 ± 5.908
	[1.1, 6.0]	$24.2 \pm 0.7 \pm 1.2$	36.482 ± 11.472	34.868 ± 5.777
		LHCb $(B^0 \to K^0\mu^+\mu^-)$ [13]		
$10^9 d\mathcal{B}/dq^2$	[0.1, 2.0]	$12.2^{+5.9}_{-5.2} \pm 0.6$	34.658 ± 10.247	32.668 ± 5.650
	[2.0, 4.0]	$18.7^{+5.5}_{-4.9} \pm 0.9$	34.073 ± 10.450	32.448 ± 6.185
	[4.0, 6.0]	$17.3^{+5.3}_{-4.8} \pm 0.9$	33.283 ± 10.899	32.034 ± 6.330
	[1.1, 6.0]	$18.7^{+3.5}_{-3.2} \pm 0.9$	33.842 ± 10.537	32.323 ± 5.907

(Table continued)

TABLE V. *(Continued)*

Observable	q^2 (GeV^2)	Experimental value	This work	*Flavio* [49]
		LHCb $(B^+ \to K^{*+}\mu^+\mu^-)$ [13]		
$10^9 d\mathcal{B}/dq^2$	[0.1, 2.0]	$59.2^{+14.4}_{-13.0} \pm 4.0$	68.174 ± 11.994	79.748 ± 10.868
	[2.0, 4.0]	$55.9^{+15.9}_{-14.4} \pm 3.8$	42.981 ± 9.597	48.903 ± 7.808
	[4.0, 6.0]	$24.9^{+11.0}_{-9.6} \pm 1.7$	47.412 ± 9.431	54.486 ± 7.912
	[1.1, 6.0]	$36.6^{+8.3}_{-7.6} \pm 2.6$	45.294 ± 9.577	51.772 ± 6.759
		LHCb $(B^0 \to K^{*0}\mu^+\mu^-)$ [14]		
$10^7 d\mathcal{B}/dq^2$	[0.10, 0.98]	$1.016^{+0.067+0.029+0.069}_{-0.073-0.029-0.069}$	0.881 ± 0.144	1.063 ± 0.146
	[1.1, 2.5]	$0.326^{+0.032+0.010+0.022}_{-0.031-0.010-0.022}$	0.405 ± 0.088	0.465 ± 0.065
	[2.5, 4.0]	$0.334^{+0.031+0.009+0.023}_{-0.033-0.009-0.023}$	0.393 ± 0.085	0.448 ± 0.062
	[4.0, 6.0]	$0.354^{+0.027+0.009+0.024}_{-0.026-0.009-0.024}$	0.435 ± 0.085	0.500 ± 0.069
	[1.0, 6.0]	$0.342^{+0.017+0.009+0.023}_{-0.017-0.009-0.023}$	0.414 ± 0.086	0.474 ± 0.073
		CMS $(B^0 \to K^{*0}\mu^+\mu^-)$ [18]		
$10^8 d\mathcal{B}/dq^2$	[1.0, 2.0]	$4.6^{+0.7}_{-0.7} \pm 0.30$	4.216 ± 0.090	4.855 ± 0.666
	[2.0, 4.30]	$3.3^{+0.5}_{-0.5} \pm 0.2$	3.939 ± 0.087	4.492 ± 0.684
	[4.30, 6.00]	$3.4^{+0.5}_{-0.5} \pm 0.3$	4.398 ± 0.086	5.056 ± 0.774
	[1.0, 6.0]	$3.6^{+0.3}_{-0.3} \pm 0.2$	4.151 ± 0.087	4.756 ± 0.716
		LHCb $(B_s^0 \to \phi\mu^+\mu^-)$ [39]		
$10^8 d\mathcal{B}/dq^2$	[0.1, 0.98]	$7.74 \pm 0.53 \pm 0.12 \pm 0.37$	10.448 ± 1.652	11.424 ± 1.236
	[1.1, 2.5]	$3.15 \pm 0.29 \pm 0.07 \pm 0.15$	4.625 ± 0.985	5.473 ± 0.610
	[2.5, 4.0]	$2.34 \pm 0.26 \pm 0.05 \pm 0.11$	4.405 ± 0.942	5.166 ± 0.662
	[4.0, 6.0]	$3.11 \pm 0.24 \pm 0.06 \pm 0.15$	4.820 ± 0.922	5.529 ± 0.788
	[1.1, 6.0]	$2.88 \pm 0.15 \pm 0.05 \pm 0.14$	4.637 ± 0.944	5.402 ± 0.559
		LHCb $(\Lambda_b^0 \to \Lambda\mu^+\mu^-)$ [59]		
$10^7 d\mathcal{B}/dq^2$	[1.1, 6.0]	$0.09^{+0.06+0.01}_{-0.05-0.01} \pm 0.02$	0.201 ± 0.064	0.136 ± 0.075
	[0.1, 2.0]	$0.36^{+0.12+0.02}_{-0.11-0.02} \pm 0.07$	0.192 ± 0.062	0.088 ± 0.053
	[2.0, 4.0]	$0.11^{+0.12+0.01}_{-0.09-0.01} \pm 0.02$	0.256 ± 0.066	0.128 ± 0.059
	[4.0, 6.0]	$0.02^{+0.09+0.01}_{-0.00-0.01} \pm 0.01$	0.213 ± 0.063	0.103 ± 0.051
		BABAR $(B \to X_S\ell^+\ell^-)$ [46]		
$10^6 d\mathcal{B}(X_s e^+e^-)/dq^2$	[1.0, 6.0]	$1.93^{+0.47+0.21}_{-0.45-0.16} \pm 0.18$	0.361 ± 0.017	0.347 ± 0.038
	[0.1, 2.0]	$3.05^{+0.52+0.29}_{-0.49-0.21} \pm 0.35$	0.779 ± 0.038	0.656 ± 0.068
	[2.0, 4.3]	$0.69^{+0.31+0.11}_{-0.28-0.07} \pm 0.07$	0.355 ± 0.017	0.345 ± 0.039
	[4.3, 6.8]	$0.69^{+0.31+0.13}_{-0.29-0.10} \pm 0.05$	0.298 ± 0.014	0.294 ± 0.033
$10^6 d\mathcal{B}(X_s\mu^+\mu^-)/dq^2$	[1.0, 6.0]	$0.66^{+0.82+0.30}_{-0.76-0.24} \pm 0.07$	0.361 ± 0.017	0.334 ± 0.032
	[0.1, 2.0]	$1.83^{+0.90+0.30}_{-0.80-0.24} \pm 0.20$	0.782 ± 0.038	0.622 ± 0.066
	[2.0, 4.3]	$-0.15^{+0.50+0.26}_{-0.43-0.14} \pm 0.01$	0.355 ± 0.017	0.331 ± 0.033
	[4.3, 6.8]	$0.34^{+0.54+0.19}_{-0.50-0.15} \pm 0.03$	0.298 ± 0.014	0.289 ± 0.029
		LHCb $(B^0 \to \ell^+\ell^-)$ [36]		
$10^9 \mathcal{B}(B_s^0 \to \mu^+\mu^-)$		$3.09^{+0.46+0.15}_{-0.43-0.11}$	3.681 ± 0.020	3.672 ± 0.152
$10^{10} \mathcal{B}(B_d^0 \to \mu^+\mu^-)$		$1.20^{+0.83+0.14}_{-0.74-0.14}$	0.997 ± 0.007	1.024 ± 0.073
		CMS $(B^0 \to \ell^+\ell^-)$ [37]		
$10^9 \mathcal{B}(B_s^0 \to \mu^+\mu^-)$		$3.83^{+0.38+0.19+0.14}_{-0.36-0.16-0.13}$	3.681 ± 0.020	3.672 ± 0.152

(Table continued)

TABLE V. *(Continued)*

Observable	q^2 (GeV^2)	Experimental value	This work	*Flavio* [49]
$10^{10}\mathcal{B}(B_d^0 \to \mu^+\mu^-)$		$0.37^{+0.75+0.08}_{-0.67-0.09}$	0.997 ± 0.007	1.024 ± 0.073
		Belle $(B \to X_s\gamma)$ [53]		
Observable	E_γ (GeV)	Experimental value	This work	*Flavio* [49]
$10^4\mathcal{B}$	>1.9	$3.51 \pm 0.17 \pm 0.33$		
10^6(EXPLT. result)	>1.6	$375 \pm 18 \pm 35$	296.1 ± 38.0	330.8 ± 22.9
		Belle $(B \to \phi\gamma)$ [54]		
Observable		Experimental value	This work	*Flavio* [49]
$10^5\mathcal{B}$		$3.6 \pm 0.5 \pm 0.3 \pm 0.6$	3.348 ± 0.526	4.072 ± 0.510

TABLE VI. The part of angular distribution observables in dataset A.

Observable	q^2 (GeV^2)	Experimental value	This work	*Flavio* [49]
		LHCb $(B_s^0 \to \phi\mu^+\mu^-)$ [40]		
F_{L}	[0.1, 0.98]	$0.254 \pm 0.045 \pm 0.017$	0.301 ± 0.060	0.345 ± 0.038
	[1.1, 4.0]	$0.723 \pm 0.053 \pm 0.015$	0.793 ± 0.044	0.811 ± 0.021
	[4.0, 6.0]	$0.701 \pm 0.050 \pm 0.016$	0.749 ± 0.050	0.750 ± 0.028
	[1.1, 6.0]	$0.715 \pm 0.036 \pm 0.013$	0.774 ± 0.047	0.785 ± 0.023
		LHCb $(B^0 \to K^{*0}\mu^+\mu^-)$ [15]		
F_L	[1.1, 6.0]	$0.700 \pm 0.025 \pm 0.013$	0.785 ± 0.050	0.750 ± 0.040
	[1.1, 2.5]	$0.655 \pm 0.046 \pm 0.017$	0.776 ± 0.051	0.760 ± 0.039
	[2.5, 4.0]	$0.756 \pm 0.047 \pm 0.023$	0.826 ± 0.043	0.797 ± 0.038
	[4.0, 6.0]	$0.684 \pm 0.035 \pm 0.015$	0.762 ± 0.054	0.712 ± 0.047
P_1	[1.1, 6.0]	$-0.079 \pm 0.159 \pm 0.021$	-0.066 ± 0.021	-0.113 ± 0.036
	[1.1, 2.5]	$-0.617 \pm 0.296 \pm 0.023$	-0.001 ± 0.001	0.024 ± 0.053
	[2.5, 4.0]	$0.168 \pm 0.371 \pm 0.043$	-0.064 ± 0.021	-0.116 ± 0.037
	[4.0, 6.0]	$0.088 \pm 0.235 \pm 0.029$	-0.103 ± 0.032	-0.178 ± 0.055
P_2	[1.1, 6.0]	$-0.162 \pm 0.050 \pm 0.012$	-0.014 ± 0.005	0.025 ± 0.085
	[1.1, 2.5]	$-0.443 \pm 0.100 \pm 0.027$	-0.452 ± 0.145	-0.451 ± 0.013
	[2.5, 4.0]	$-0.191 \pm 0.116 \pm 0.043$	-0.114 ± 0.033	-0.064 ± 0.101
	[4.0, 6.0]	$0.105 \pm 0.068 \pm 0.009$	0.268 ± 0.086	0.293 ± 0.074
P_3	[1.1, 6.0]	$0.085 \pm 0.090 \pm 0.005$	0.001 ± 0.0004	0.003 ± 0.010
	[1.1, 2.5]	$0.324 \pm 0.147 \pm 0.014$	0.001 ± 0.001	0.004 ± 0.021
	[2.5, 4.0]	$0.049 \pm 0.195 \pm 0.014$	0.002 ± 0.001	0.004 ± 0.010
	[4.0, 6.0]	$-0.090 \pm 0.139 \pm 0.006$	0.001 ± 0.0004	0.003 ± 0.017
P_4'	[1.1, 6.0]	$-0.298 \pm 0.087 \pm 0.016$	-0.338 ± 0.090	-0.353 ± 0.040
	[1.1, 2.5]	$-0.080 \pm 0.142 \pm 0.019$	-0.056 ± 0.016	-0.061 ± 0.044
	[2.5, 4.0]	$-0.435 \pm 0.169 \pm 0.035$	-0.374 ± 0.101	-0.392 ± 0.044
	[4.0, 6.0]	$-0.312 \pm 0.115 \pm 0.013$	-0.489 ± 0.122	-0.503 ± 0.029
P_5'	[1.1, 6.0]	$-0.114 \pm 0.068 \pm 0.026$	-0.406 ± 0.110	-0.447 ± 0.096
	[1.1, 2.5]	$0.365 \pm 0.122 \pm 0.013$	0.208 ± 0.055	0.139 ± 0.075
	[2.5, 4.0]	$-0.150 \pm 0.144 \pm 0.032$	-0.451 ± 0.126	-0.501 ± 0.102
	[4.0, 6.0]	$-0.439 \pm 0.111 \pm 0.036$	-0.752 ± 0.191	-0.759 ± 0.069

(Table continued)

TABLE VI. *(Continued)*

Observable	q^2 (GeV^2)	Experimental value	This work	*Flavio* [49]
P_6'	[1.1, 6.0]	$-0.197 \pm 0.075 \pm 0.009$	-0.045 ± 0.011	-0.046 ± 0.117
	[1.1, 2.5]	$-0.226 \pm 0.128 \pm 0.005$	-0.068 ± 0.018	-0.069 ± 0.083
	[2.5, 4.0]	$-0.155 \pm 0.148 \pm 0.024$	-0.051 ± 0.013	-0.052 ± 0.106
	[4.0, 6.0]	$-0.293 \pm 0.117 \pm 0.004$	-0.028 ± 0.007	-0.030 ± 0.121
P_8'	[1.1, 6.0]	$-0.020 \pm 0.089 \pm 0.009$	-0.013 ± 0.003	-0.015 ± 0.031
	[1.1, 2.5]	$-0.366 \pm 0.158 \pm 0.005$	-0.015 ± 0.004	-0.018 ± 0.037
	[2.5, 4.0]	$0.037 \pm 0.169 \pm 0.007$	-0.016 ± 0.004	-0.017 ± 0.038
	[4.0, 6.0]	$0.166 \pm 0.127 \pm 0.004$	-0.010 ± 0.002	-0.012 ± 0.032
		CMS $(B^0 \to K^{*0}\mu^+\mu^-)$ [19]		
P_1	[1.0, 2.0]	$0.12^{+0.46}_{-0.47} \pm 0.10$	0.007 ± 0.002	0.045 ± 0.053
	[2.0, 4.30]	$-0.69^{+0.58}_{-0.27} \pm 0.023$	-0.059 ± 0.020	-0.105 ± 0.037
	[4.30, 6.00]	$0.53^{+0.24}_{-0.33} \pm 0.19$	-0.104 ± 0.033	-0.180 ± 0.048
P_5'	[1.0, 2.0]	$0.10^{+0.32}_{-0.31} \pm 0.07$	0.352 ± 0.101	0.289 ± 0.061
	[2.0, 4.30]	$-0.57^{+0.34}_{-0.31} \pm 0.18$	-0.398 ± 0.108	-0.450 ± 0.099
	[4.30, 6.00]	$-0.96^{+0.22}_{-0.21} \pm 0.25$	-0.766 ± 0.191	-0.771 ± 0.077
		CMS $(B^0 \to K^{*0}\mu^+\mu^-)$ [18]		
F_L	[1.0, 2.0]	$0.64^{+0.10}_{-0.09} \pm 0.07$	0.739 ± 0.057	0.724 ± 0.052
	[2.0, 4.30]	$0.80^{+0.08}_{-0.08} \pm 0.06$	0.822 ± 0.043	0.794 ± 0.034
	[4.30, 6.00]	$0.62^{+0.10}_{-0.09} \pm 0.07$	0.756 ± 0.054	0.704 ± 0.055
	[1.0, 6.0]	$0.73^{+0.05}_{-0.05} \pm 0.04$	0.781 ± 0.050	0.747 ± 0.042
A_{FB}	[1.0, 2.0]	$-0.27^{+0.17}_{-0.40} \pm 0.07$	-0.143 ± 0.038	-0.156 ± 0.033
	[2.0, 4.30]	$-0.12^{+0.15}_{-0.17} \pm 0.05$	-0.034 ± 0.009	-0.026 ± 0.029
	[4.30, 6.00]	$0.01^{+0.15}_{-0.15} \pm 0.03$	0.100 ± 0.024	0.132 ± 0.039
	[1.0, 6.0]	$-0.16^{+0.10}_{-0.09} \pm 0.05$	-0.008 ± 0.002	0.005 ± 0.030
		ATLAS $(B^0 \to K^{*0}\mu^+\mu^-)$ [17]		
F_{L}	[2.0, 4.0]	$0.64^{+0.11}_{-0.11} \pm 0.05$	0.825 ± 0.042	0.799 ± 0.036
	[4.0, 6.0]	$0.42^{+0.13}_{-0.13} \pm 0.12$	0.762 ± 0.053	0.712 ± 0.048
	[1.1, 6.0]	$0.56^{+0.07}_{-0.07} \pm 0.06$	0.785 ± 0.050	0.750 ± 0.038
P_1	[2.0, 4.0]	$-0.78^{+0.51}_{-0.51} \pm 0.34$	-0.053 ± 0.018	-0.095 ± 0.039
	[4.0, 6.0]	$0.14^{+0.43}_{-0.43} \pm 0.26$	-0.103 ± 0.033	-0.178 ± 0.051
	[1.1, 6.0]	$-0.17^{+0.31}_{-0.31} \pm 0.13$	-0.066 ± 0.022	-0.113 ± 0.033
P_4'	[2.0, 4.0]	$-0.76^{+0.31}_{-0.31} \pm 0.21$	-0.330 ± 0.088	-0.347 ± 0.044
	[4.0, 6.0]	$0.64^{+0.33}_{-0.33} \pm 0.18$	-0.489 ± 0.125	-0.503 ± 0.028
	[1.1, 6.0]	$0.05^{+0.22}_{-0.22} \pm 0.14$	-0.338 ± 0.088	-0.353 ± 0.034
P_5'	[2.0, 4.0]	$-0.33^{+0.31}_{-0.31} \pm 0.13$	-0.353 ± 0.096	-0.410 ± 0.107
	[4.0, 6.0]	$0.26^{+0.35}_{-0.35} \pm 0.18$	-0.752 ± 0.196	-0.759 ± 0.082
	[1.1, 6.0]	$0.01^{+0.21}_{-0.21} \pm 0.08$	-0.406 ± 0.108	-0.447 ± 0.092
P_6'	[2.0, 4.0]	$0.31^{+0.28}_{-0.28} \pm 0.19$	-0.055 ± 0.014	-0.056 ± 0.099
	[4.0, 6.0]	$0.06^{+0.27}_{-0.27} \pm 0.13$	-0.028 ± 0.006	-0.030 ± 0.129
	[1.1, 6.0]	$0.03^{+0.17}_{-0.17} \pm 0.12$	-0.045 ± 0.011	-0.046 ± 0.088

(Table continued)

TABLE VI. *(Continued)*

Observable	q^2 (GeV^2)	Experimental value	This work	*Flavio* [49]
P_8'	[2.0, 4.0]	$1.07^{+0.41}_{-0.41} \pm 0.39$	-0.016 ± 0.004	-0.018 ± 0.037
	[4.0, 6.0]	$-0.24^{+0.42}_{-0.42} \pm 0.09$	-0.010 ± 0.002	-0.012 ± 0.032
	[1.1, 6.0]	$0.23^{+0.28}_{-0.28} \pm 0.20$	-0.013 ± 0.003	-0.015 ± 0.037
		Belle ($B^0 \to K^{*0} e^+ e^-$) [7]		
$P_4^{\mu'}$	[1.0, 6.0]	$-0.22^{+0.35}_{-0.34} \pm 0.15$	-0.326 ± 0.086	-0.341 ± 0.045
	[0.10, 4.00]	$-0.38^{+0.50}_{-0.48} \pm 0.12$	-0.026 ± 0.008	-0.028 ± 0.030
	[4.00, 8.00]	$-0.07^{+0.32}_{-0.31} \pm 0.07$	-0.503 ± 0.124	-0.518 ± 0.026
$P_4^{e'}$	[1.0, 6.0]	$-0.72^{+0.40}_{-0.39} \pm 0.06$	-0.323 ± 0.093	-0.338 ± 0.037
	[0.10, 4.00]	$0.34^{+0.41}_{-0.45} \pm 0.11$	-0.004 ± 0.002	-0.004 ± 0.030
	[4.00, 8.00]	$-0.52^{+0.24}_{-0.22} \pm 0.03$	-0.503 ± 0.124	-0.518 ± 0.021
$P_5^{\mu'}$	[1.0, 6.0]	$0.43^{+0.26}_{-0.28} \pm 0.10$	-0.382 ± 0.104	-0.423 ± 0.082
	[0.10, 4.00]	$0.42^{+0.39}_{-0.39} \pm 0.14$	0.205 ± 0.061	0.156 ± 0.064
	[4.00, 8.00]	$-0.03^{+0.31}_{-0.30} \pm 0.09$	-0.802 ± 0.198	-0.795 ± 0.070
$P_5^{e'}$	[1.0, 6.0]	$-0.22^{+0.39}_{-0.41} \pm 0.03$	-0.375 ± 0.107	-0.416 ± 0.092
	[0.10, 4.00]	$0.51^{+0.39}_{-0.46} \pm 0.09$	0.219 ± 0.063	0.174 ± 0.063
	[4.00, 8.00]	$-0.52^{+0.28}_{-0.26} \pm 0.03$	-0.799 ± 0.197	-0.792 ± 0.057
Q_4	[1.0, 6.0]	$0.498^{+0.527}_{-0.527} \pm 0.166$	-0.003 ± 0.127	-0.003 ± 0.0002
	[0.10, 4.00]	$-0.723^{+0.676}_{-0.676} \pm 0.163$	-0.022 ± 0.008	-0.024 ± 0.003
	[4.00, 8.00]	$0.448^{+0.392}_{-0.392} \pm 0.076$	-0.000 ± 0.175	-0.000 ± 0.000
Q_5	[1.0, 6.0]	$0.656^{+0.485}_{-0.485} \pm 0.103$	-0.007 ± 0.149	-0.007 ± 0.001
	[0.10, 4.00]	$-0.097^{+0.601}_{-0.601} \pm 0.164$	-0.014 ± 0.088	-0.018 ± 0.006
	[4.00, 8.00]	$0.498^{+0.410}_{-0.410} \pm 0.095$	-0.003 ± 0.279	-0.003 ± 0.000
		LHCb ($B^+ \to K^{*+} \mu^+ \mu^-$) [16]		
F_L	[1.1, 2.5]	$0.54^{+0.18}_{-0.19} \pm 0.03$	0.784 ± 0.049	0.768 ± 0.041
	[2.5, 4.0]	$0.17^{+0.24}_{-0.14} \pm 0.04$	0.829 ± 0.042	0.800 ± 0.034
	[4.0, 6.0]	$0.67^{+0.11}_{-0.14} \pm 0.03$	0.764 ± 0.053	0.714 ± 0.051
	[1.1, 6.0]	$0.59^{+0.10}_{-0.10} \pm 0.03$	0.788 ± 0.049	0.754 ± 0.038
P_1	[1.1, 2.5]	$1.60^{+4.92}_{-1.75} \pm 0.32$	-0.001 ± 0.0004	0.022 ± 0.049
	[2.5, 4.0]	$-0.29^{+1.43}_{-1.04} \pm 0.22$	-0.064 ± 0.021	-0.118 ± 0.036
	[4.0, 6.0]	$-1.24^{+0.99}_{-1.17} \pm 0.29$	-0.102 ± 0.032	-0.178 ± 0.049
	[1.1, 6.0]	$-0.51^{+0.56}_{-0.54} \pm 0.08$	-0.066 ± 0.022	-0.115 ± 0.032
P_2	[1.1, 2.5]	$-0.28^{+0.24}_{-0.42} \pm 0.15$	-0.453 ± 0.154	-0.451 ± 0.016
	[2.5, 4.0]	$0.03^{+0.26}_{-0.25} \pm 0.11$	-0.109 ± 0.033	-0.055 ± 0.107
	[4.0, 6.0]	$-0.15^{+0.19}_{-0.20} \pm 0.06$	0.268 ± 0.087	0.295 ± 0.064
	[1.1, 6.0]	$-0.13^{+0.13}_{-0.13} \pm 0.05$	-0.011 ± 0.005	0.032 ± 0.080
P_3	[1.1, 2.5]	$-0.09^{+0.70}_{-0.99} \pm 0.18$	0.001 ± 0.0004	0.004 ± 0.021
	[2.5, 4.0]	$-0.45^{+0.50}_{-0.62} \pm 0.20$	0.002 ± 0.0005	0.004 ± 0.011
	[4.0, 6.0]	$0.52^{+0.82}_{-0.62} \pm 0.15$	0.001 ± 0.0004	0.003 ± 0.014
	[1.1, 6.0]	$0.12^{+0.27}_{-0.28} \pm 0.04$	0.001 ± 0.0004	0.003 ± 0.010

(Table continued)

TABLE VI. *(Continued)*

Observable	q^2 (GeV^2)	Experimental value	This work	*Flavio* [49]
P_4'	[1.1, 2.5]	$0.58^{+0.62}_{-0.56} \pm 0.11$	-0.052 ± 0.015	-0.063 ± 0.043
	[2.5, 4.0]	$-0.81^{+1.09}_{-0.84} \pm 0.14$	-0.371 ± 0.098	-0.391 ± 0.044
	[4.0, 6.0]	$-0.79^{+0.47}_{-0.28} \pm 0.09$	-0.487 ± 0.120	-0.502 ± 0.027
	[1.1, 6.0]	$-0.41^{+0.28}_{-0.28} \pm 0.07$	-0.335 ± 0.096	-0.353 ± 0.042
P_5'	[1.1, 2.5]	$0.88^{+0.70}_{-0.71} \pm 0.10$	0.180 ± 0.050	0.113 ± 0.113
	[2.5, 4.0]	$-0.87^{+1.00}_{-1.68} \pm 0.09$	-0.467 ± 0.125	-0.517 ± 0.098
	[4.0, 6.0]	$-0.25^{+0.32}_{-0.40} \pm 0.09$	-0.756 ± 0.187	-0.764 ± 0.083
	[1.1, 6.0]	$-0.07^{+0.25}_{-0.25} \pm 0.04$	-0.421 ± 0.123	-0.461 ± 0.086
P_6'	[1.1, 2.5]	$0.25^{+1.22}_{-1.32} \pm 0.08$	-0.059 ± 0.017	-0.054 ± 0.083
	[2.5, 4.0]	$-0.37^{+1.59}_{-3.91} \pm 0.05$	-0.049 ± 0.012	-0.044 ± 0.102
	[4.0, 6.0]	$-0.09^{+0.40}_{-0.41} \pm 0.05$	-0.029 ± 0.007	-0.028 ± 0.113
	[1.1, 6.0]	$-0.21^{+0.23}_{-0.23} \pm 0.04$	-0.043 ± 0.012	-0.039 ± 0.092
P_8'	[1.1, 2.5]	$0.12^{+0.75}_{-0.76} \pm 0.05$	-0.021 ± 0.005	-0.027 ± 0.040
	[2.5, 4.0]	$0.12^{+7.89}_{-4.95} \pm 0.07$	-0.016 ± 0.004	-0.018 ± 0.034
	[4.0, 6.0]	$-0.15^{+0.44}_{-0.48} \pm 0.05$	-0.011 ± 0.002	-0.011 ± 0.033
	[1.1, 6.0]	$0.03^{+0.26}_{-0.28} \pm 0.06$	-0.015 ± 0.004	-0.017 ± 0.036
		LHCb $(B^0 \to K^{*0} e^+ e^-)$ [38]		
F_L	[0.0008, 0.257]	$0.044 \pm 0.026 \pm 0.014$	0.077 ± 0.026	0.050 ± 0.013
$A_T^{\Re}$	[0.0008, 0.257]	$-0.06 \pm 0.08 \pm 0.02$	-0.032 ± 0.012	-0.024 ± 0.001
A_T^2	[0.0008, 0.257]	$0.11 \pm 0.10 \pm 0.02$	-0.000 ± 0.000	-0.002 ± 0.021
$A_T^{\Im}$	[0.0008, 0.257]	$0.02 \pm 0.10 \pm 0.01$	0.001 ± 0.000	0.032 ± 0.020
		LHCb $(B_s^0 \to \phi\gamma)$ [56]		
$S_{\phi\gamma}$		$0.43 \pm 0.30 \pm 0.11$	0.001 ± 0.000	-0.000 ± 0.0002
A_{CP}		$0.11 \pm 0.29 \pm 0.11$	0.000 ± 0.000	0.004 ± 0.002
$A_{\Delta\Gamma}$		$-0.67^{+0.37}_{-0.41} \pm 0.17$	0.029 ± 0.000	0.031 ± 0.020

TABLE VII. The updated components related to LHCb new results in dataset B, where the branching fractions are in the unit of GeV^{-2}.

		LHCb $(B \to K^{(*)} \ell^+ \ell^-)$ [20]		
Observable	q^2 (GeV^2)	Experimental value	This work	*Flavio* [49]
R_K	[0.1, 1.1]	$0.994^{+0.090+0.029}_{-0.082-0.027}$	0.994 ± 0.000	0.993 ± 0.000
R_K	[1.1, 6.0]	$0.949^{+0.042+0.022}_{-0.041-0.022}$	1.000 ± 0.000	1.001 ± 0.000
R_{K^*}	[0.1, 1.1]	$0.927^{+0.093+0.036}_{-0.087-0.035}$	0.983 ± 0.000	0.983 ± 0.001
R_{K^*}	[1.1, 6.0]	$1.027^{+0.072+0.027}_{-0.068-0.026}$	0.996 ± 0.000	0.996 ± 0.001
$10^9 d\mathcal{B}(K^+ e^+ e^-)/dq^2$	[1.1, 6.0]	$25.5^{+1.3}_{-1.2} \pm 1.1$	36.474 ± 11.5	34.841 ± 6.065
$10^9 d\mathcal{B}(K^{*0} e^+ e^-)/dq^2$	[1.1, 6.0]	$33.3^{+2.7}_{-2.6} \pm 2.2$	41.541 ± 8.73	47.580 ± 7.031

[1] J. T. Wei *et al.* (Belle Collaboration), Phys. Rev. Lett. **103**, 171801 (2009).
[2] B. Aubert *et al.* (*BABAR* Collaboration), Phys. Rev. D **79**, 031102 (2009).
[3] T. Aaltonen *et al.* (CDF Collaboration), Phys. Rev. Lett. **106**, 161801 (2011).
[4] R. Aaij *et al.* (LHCb Collaboration), Phys. Rev. Lett. **108**, 181806 (2012).
[5] A. Abdesselam *et al.* (Belle Collaboration), Phys. Rev. Lett. **126**, 161801 (2021).
[6] S. Choudhury *et al.* (BELLE Collaboration), J. High Energy Phys. 03 (2021) 105.
[7] S. Wehle *et al.* (Belle Collaboration), Phys. Rev. Lett. **118**, 111801 (2017).
[8] R. Aaij *et al.* (LHCb Collaboration), Phys. Rev. Lett. **113**, 151601 (2014).
[9] R. Aaij *et al.* (LHCb Collaboration), Phys. Rev. Lett. **122**, 191801 (2019).
[10] R. Aaij *et al.* (LHCb Collaboration), Nat. Phys. **18**, 277 (2022).
[11] R. Aaij *et al.* (LHCb Collaboration), Phys. Rev. Lett. **128**, 191802 (2022).
[12] R. Aaij *et al.* (LHCb Collaboration), J. High Energy Phys. 08 (2017) 055.
[13] R. Aaij *et al.* (LHCb Collaboration), J. High Energy Phys. 06 (2014) 133.
[14] R. Aaij *et al.* (LHCb Collaboration), J. High Energy Phys. 11 (2016) 047; 04 (2017) 142(E).
[15] R. Aaij *et al.* (LHCb Collaboration), Phys. Rev. Lett. **125**, 011802 (2020).
[16] R. Aaij *et al.* (LHCb Collaboration), Phys. Rev. Lett. **126**, 161802 (2021).
[17] M. Aaboud *et al.* (ATLAS Collaboration), J. High Energy Phys. 10 (2018) 047.
[18] V. Khachatryan *et al.* (CMS Collaboration), Phys. Lett. B **753**, 424 (2016).
[19] A. M. Sirunyan *et al.* (CMS Collaboration), Phys. Lett. B **781**, 517 (2018).
[20] LHCb Collaboration, Phys. Rev. D **108**, 032002 (2023).
[21] M. Beneke, T. Feldmann, and D. Seidel, Eur. Phys. J. C **41**, 173 (2005).
[22] M. Beneke, T. Feldmann, and D. Seidel, Nucl. Phys. **B612**, 25 (2001).
[23] M. Algueró, B. Capdevila, S. Descotes-Genon, J. Matias, and M. Novoa-Brunet, Eur. Phys. J. C **82**, 326 (2022).
[24] W. Altmannshofer and P. Stangl, Eur. Phys. J. C **81**, 952 (2021).
[25] T. Hurth, F. Mahmoudi, D. Martinez Santos, and S. Neshatpour, Springer Proc. Phys. **292**, 11 (2023).
[26] L.-S. Geng, B. Grinstein, S. Jäger, S.-Y. Li, J. Martin Camalich, and R.-X. Shi, Phys. Rev. D **104**, 035029 (2021).
[27] F. Munir Bhutta, Z.-R. Huang, C.-D. Lü, M. A. Paracha, and W. Wang, Nucl. Phys. **B979**, 115763 (2022).
[28] N. Gubernari, M. Reboud, D. van Dyk, and J. Virto, J. High Energy Phys. 09 (2022) 133.
[29] N. R. Singh Chundawat, Phys. Rev. D **107**, 075014 (2023).
[30] W. Altmannshofer, P. Ball, A. Bharucha, A. J. Buras, D. M. Straub, and M. Wick, J. High Energy Phys. 01 (2009) 019.
[31] D. Du, A. X. El-Khadra, S. Gottlieb, A. S. Kronfeld, J. Laiho, E. Lunghi, R. S. Van de Water, and R. Zhou, Phys. Rev. D **93**, 034005 (2016).
[32] W.-S. Hou, M. Kohda, and F. Xu, Phys. Rev. D **90**, 013002 (2014).
[33] T. Blake, G. Lanfranchi, and D. M. Straub, Prog. Part. Nucl. Phys. **92**, 50 (2017).
[34] A. Biswas, S. Nandi, S. K. Patra, and I. Ray, Nucl. Phys. **B969**, 115479 (2021).
[35] C. Bobeth, T. Ewerth, F. Kruger, and J. Urban, Phys. Rev. D **64**, 074014 (2001).
[36] R. Aaij *et al.* (LHCb Collaboration), Phys. Rev. D **105**, 012010 (2022).
[37] CMS Collaboration, Phys. Lett. B **842**, 137955 (2023).
[38] R. Aaij *et al.* (LHCb Collaboration), J. High Energy Phys. 12 (2020) 081.
[39] R. Aaij *et al.* (LHCb Collaboration), Phys. Rev. Lett. **127**, 151801 (2021).
[40] R. Aaij *et al.* (LHCb Collaboration), J. High Energy Phys. 11 (2021) 043.
[41] F. Mahmoudi, Comput. Phys. Commun. **180**, 1579 (2009).
[42] Y.-B. Dai, C.-S. Huang, and H.-W. Huang, Phys. Lett. B **390**, 257 (1997); **513**, 429(E) (2001).
[43] A. Ghinculov, T. Hurth, G. Isidori, and Y. P. Yao, Nucl. Phys. **B685**, 351 (2004).
[44] T. Huber, T. Hurth, J. Jenkins, E. Lunghi, Q. Qin, and K. K. Vos, J. High Energy Phys. 10 (2020) 088.
[45] T. Huber, T. Hurth, J. Jenkins, and E. Lunghi, arXiv:2306.03134.
[46] J. P. Lees *et al.* (*BABAR* Collaboration), Phys. Rev. Lett. **112**, 211802 (2014).
[47] M. Misiak *et al.*, Phys. Rev. Lett. **98**, 022002 (2007).
[48] M. Misiak and M. Steinhauser, Nucl. Phys. **B764**, 62 (2007).
[49] D. M. Straub, arXiv:1810.08132.
[50] P. Gambino and C. Schwanda, Phys. Rev. D **89**, 014022 (2014).
[51] A. Paul and D. M. Straub, J. High Energy Phys. 04 (2017) 027.
[52] F. Muheim, Y. Xie, and R. Zwicky, Phys. Lett. B **664**, 174 (2008).
[53] T. Saito *et al.* (Belle Collaboration), Phys. Rev. D **91**, 052004 (2015).
[54] D. Dutta *et al.* (Belle Collaboration), Phys. Rev. D **91**, 011101 (2015).
[55] F. Abudinén *et al.* (Belle II Collaboration), arXiv:2110.08219.
[56] R. Aaij *et al.* (LHCb Collaboration), Phys. Rev. Lett. **123**, 081802 (2019).
[57] P. Böer, T. Feldmann, and D. van Dyk, J. High Energy Phys. 01 (2015) 155.
[58] W. Detmold and S. Meinel, Phys. Rev. D **93**, 074501 (2016).
[59] R. Aaij *et al.* (LHCb Collaboration), J. High Energy Phys. 06 (2015) 115; 09 (2018) 145(E).
[60] M. Ciuchini, M. Fedele, E. Franco, A. Paul, L. Silvestrini, and M. Valli, Phys. Rev. D **107**, 055036 (2023).
[61] M. Ciuchini, M. Fedele, E. Franco, A. Paul, L. Silvestrini, and M. Valli, Phys. Rev. D **103**, 015030 (2021).

[62] M. Ciuchini, A. M. Coutinho, M. Fedele, E. Franco, A. Paul, L. Silvestrini, and M. Valli, Eur. Phys. J. C **79**, 719 (2019).
[63] K. Kowalska, D. Kumar, and E. M. Sessolo, Eur. Phys. J. C **79**, 840 (2019).
[64] R. L. Workman *et al.* (Particle Data Group Collaboration), Prog. Theor. Exp. Phys. **2022**, 083C01 (2022).
[65] C. Bobeth, M. Gorbahn, T. Hermann, M. Misiak, E. Stamou, and M. Steinhauser, Phys. Rev. Lett. **112**, 101801 (2014).
[66] M. J. Aslam, Y.-M. Wang, and C.-D. Lu, Phys. Rev. D **78**, 114032 (2008).
[67] F. Abudinén *et al.* (Belle-II Collaboration), arXiv:2111.09405.
[68] C. Bobeth, G. Hiller, D. van Dyk, and C. Wacker, J. High Energy Phys. 01 (2012) 107.
[69] A. Bharucha, D. M. Straub, and R. Zwicky, J. High Energy Phys. 08 (2016) 098.
[70] E. E. Jenkins, A. V. Manohar, and P. Stoffer, J. High Energy Phys. 03 (2018) 016.
[71] O. Catà and M. Jung, Phys. Rev. D **92**, 055018 (2015).
[72] K. De Bruyn, R. Fleischer, R. Knegjens, P. Koppenburg, M. Merk, A. Pellegrino, and N. Tuning, Phys. Rev. Lett. **109**, 041801 (2012).
[73] C. Greub, V. Pilipp, and C. Schupbach, J. High Energy Phys. 12 (2008) 040.
[74] A. Khodjamirian, T. Mannel, A. A. Pivovarov, and Y. M. Wang, J. High Energy Phys. 09 (2010) 089.
[75] N. Gubernari, D. van Dyk, and J. Virto, J. High Energy Phys. 02 (2021) 088.
[76] G. Burdman and G. Hiller, Phys. Rev. D **63**, 113008 (2001).
[77] C. Bobeth, G. Hiller, and G. Piranishvili, J. High Energy Phys. 12 (2007) 040.